FACULTY OF SCIENCE AND TECHNOLOGY

MASTER'S THESIS

Study program/specialization:
Marine and Offshore Technology

The autumn semester, 2023
Open / Confidential

Author:
Terry Zahi

Main supervisor:
Muk Chen Ong

Co-supervisor:
Xueliang Wen

Thesis title:
Dynamic Analysis of Floating Dock Operations with Corrosion-induced Holes at Ballast Tanks

Credits (ECTS): 30

i

Acknowledgement

To begin with, I want to express my deepest thanks to Professor Muk Chen Ong, my main supervisor for his genuine support, motivation, and valuable advice. Under his guidance, I have achieved more and found motivation to succeed in both my academic journey and professional pursuits.

I would also like to commend my co-supervisor Xueliang Wen, for his assistance and guidance. I have learnt a lot from him and for that I am entirely grateful.

A special thanks goes to the University of Stavanger, specifically the Marine and offshore department for providing me with the resources needed to compete my studies.

To conclude, my final thanks go to my family, who have supported me throughout my masters studies. Without them this would not be possible.

Abstract

The corrosion at the ballast tanks is a concern risk for floating docks that have been in service for several decades. Corrosion events can result in severe accidents and huge economic costs. To migrate the corrosion risk, the dynamic response of a floating dock under corrosion-induced accidents are studied using a numerical method. The numerical model is proposed to calculate the dynamic responses of the floating dock during operations. It includes a six-degree-of-freedom (6-DOF) model, a hydrostatic force model, a hydrodynamic force model, a hydraulic model and a modified P-controller. The hydraulic model is proposed to model the flow through the valves and pumps as well as the corrosion-induced holes. The investigated floating dock is equipped with 18 ballast tanks, which are exposed to corrosion due to the seawater. The influence of the position and the diameter of the corrosion-induced holes on the stability and the dynamic behavours of the floating dock at its work position and during the ballasting and de-balllasting operation are studied numerically using the proposed model. For the corrosion-induced ballasting of the floating dock at its working position, the maximum pitch and roll angles are 0.42 degrees and 2.04 degrees respectively when there are one or two holes located at different tanks. For the automatic ballasting with corrosion-induced holes, the maximum roll and pitch angles during the operations are found proportional to hole diameters. With two 300 mm-diameter corrosion-induced holes at different ballast tanks, the present modified P-controller is able to regulate the floating dock's pitch and roll angles within very small ranges. For the automatic de-ballasting with corrosion-induced holes with a diameter of 300mm, the presence of automatic ballast control couldn't keep all cases within a safe margin because some special locations of the corrosion-induced holes cause large trim and roll moments. This analysis can emphasize potential hazards of the corrosion-induced holes, and presents an opportunity for the maritime sector to enhance safety, operational efficiency, and environmental responsibility.

Table of Contents

List of Tables

List of Figures

1 Introduction

1.1   Motivation and background

A floating dock is a ship-repairing platform [1] on which the damaged ship and its steel structure below the waterline can be conveniently repaired, as shown in Figures 1 and 2. It comprises a floating platform with a pontoon deck, two lateral barriers known as wing walls, and multiple ballast tanks. The pontoon serves as the primary supporting structure responsible for displacing the weight of both the vessel and the dry dock, facilitating the lifting of marine floating vessels through buoyancy. To achieve this, the transverse strength of the pontoon must be able to endure the load exerted by the ship, which is typically concentrated along the centerline of the dock, while also providing consistent buoyant support against water pressure. The inclusion of wing walls is advantageous for maintaining stability when the pontoon is submerged and for ensuring its longitudinal strength, especially when faced with the non-uniform weight distribution of the ship and the not even buoyant support [2].Floating docks are an essential component of the maritime sector's infrastructure, acting as adaptable work platforms for a range of nautical activities, such as ship maintenance, repair, and building. For ports and shipyards to operate effectively, floating docks must be designed, built, and operated effectively.

According to the report of Anish Wankhede [3], floating dock can be propelled to the location of a salvage vessel near the harbor. They are more cost-effective to upkeep in comparison to graving docks and offer a greater potential for resale value. Additionally, they can be positioned either near or at a distance from the shoreline within the harbor, thus serving as a mobile and compact structure that doesn't encroach upon the space of the shore facility.

The hydraulic components provide precise control over the inflow and outflow of water during these processes, allowing for accurate adjustments to the dock's draught, trim, and heel. This control is essential for the safe and efficient loading and unloading of vessels on the floating dock. It consists of pumps, pipes, tanks and valves. The purpose of the valves is to control the flow of water into or out of the ballast tanks.When a ballast tank is open to the sea, it is usually positioned below the waterline of a ship or dock, hence,the water flows into the ballast tanks due to gravity. The pump pressure is not required to push the water into the ballast. It can help reduce the operation cost of the shipyard. The water inside the tank rises to a specific level where the inner water head is equal to that of the surrounding water. As water flows into the tanks, it increases the weight of

the dock, causing it to sink to a desired draught. This is termed as ballasting. This controlled sinking helps make the dock deck below the water surface, enabling vessels to enter smoothly. On the other hand, during de-ballasting operation, a pump is frequently needed to counteract the hydrostatic pressure outside the dock. A single pump can be used to de-ballast more than one ballast tanks located inside floating dock. As the water in the ballast tank is expelled, there tends to be a reduction in the dock's weight and this causes it to rise back to its working position.

Figure 1. Ship construction on a floating dock in Klaipeda, Lithuania [4]

1.2 State of the Art

Despite their essential role, floating docks are far from impervious to the relentless challenges posed by various hazards. Below are a few explained hazards further explained.

1.2.1 Topographical hazards

Selecting the right location in the initial planning phase is the primary step to ensure the secure operation of a floating dock. The geographical location of a shipyard significantly influences where the floating dock should be placed. Factors such as water depth, proximity to neighboring shipyards,

local maritime traffic, and environmental conditions, like susceptibility to typhoons, seismic events, and tsunamis, are all factors taken into account when deciding on the suitable site. In two instances within South-East Asia [5], The side shell plates, securing piles, and ramps of floating docks have experienced corrosion damage due to the waves produced by passing vessels. The first instance involved a vessel returning from a sea trial, moving at high speed near a moored floating dock in a neighboring shipyard. The wake created by this passing vessel led to significant rolling of the floating dock, causing notable damage to its piles.

In the second scenario, a jack-up barge was being deployed from the shoreline of a shipyard, while a floating dock was positioned on the opposite side of the basin [6]. As the barge was launched, it caused substantial waves that surged across the basin, resulting in damage to the side shell plates and piles of the floating dock. Shipyards in busy maritime centers such as Singapore are frequently situated near one another, heightening the risks associated with passing vessels and ship-launching activities, posing significant concerns for potential hazards. Likewise, floating docks situated in regions prone to tsunamis encounter increased risks. Despite having early warnings for tsunamis, moving a floating dock is a time-intensive procedure that requires several sequential steps [7]. The process involves unloading the dock, disengaging the locking system and ramps, stowing the cranes, and ensuring the availability of suitable towing gear and tugs for the relocation.

Figure 2. Floating dock in an accidental condition at Tuzla Ship Repair Yard [8].

Shipyards located along riverbanks or in shallow waters often encounter the necessity of regularly towing the floating dock to deeper waters for docking operations. This introduces additional risks, including managing challenging currents, the possibility of collisions with other vessels, and the risk of grounding while relocating the dock.

1.2.2   Operational Hazards

The most crucial stage in the operation of a floating dock is when it begins de-ballasting to hoist a vessel out of the water for docking. It's essential to accurately assess the vessel's weight and center of gravity. Inaccurate data or estimations regarding these factors can cause excessive trim and/or list, and in severe situations, a loss of positive stability, potentially resulting in the sinking of both the floating dock and the docking vessel. Hence, meticulous monitoring of the floating dock's stability is crucial throughout the docking procedure.

A submerged floating dock has limited reserve resilience, and its relatively small waterplane area from the wing walls makes it susceptible to unintended weight shifts or incorrect ballasting sequences. Malfunctions in remotely operated valves or ballast pumps can create uneven ballasting conditions, leading to excessive trimming, increased stress on the floating dock, and the potential for damaging impacts or rapid, excessive trim and list. This could ultimately compromise buoyancy, resulting in the sinking of the dock.

During a docking operation, a floating dock sank in a particular incident due to excessive trim resulting from the failure of ballast valves, which had corroded. This excessive trim caused the aft vent pipe openings to submerge, causing swift flooding of compartments and ultimately resulting in the sinking of the floating dock at its berth [6]. In a separate incident, a floating dock sank because the keel blocks were inaccurately positioned. As the floating dock lifted the vessel from the water, several keel blocks pierced the pontoon deck, leading to flooding in multiple ballast tanks. This rapid influx of water resulted in a swift loss of buoyancy, ultimately causing the floating dock to sink [9].

Moreover, the cranes located high on the side wall top deck of the floating dock are vulnerable to strong winds, increasing the risk of tipping over during severe weather conditions or sudden squalls [10]. Within the Sumatra, Malaysia, and Singapore region, a weather phenomenon called Sumatran Squalls occurs, usually occurring between 200 hours and 500 hours, characterized by winds reaching gusts of up to 50 knots [11]. Amid these squalls, floating docks face potential

incidents like crane toppling or mooring line failure. To reduce this risk, it's crucial for floating docks to ensure that all cranes are correctly stowed, with their booms securely resting in their home position when they are not in use.

1.2.3 Corrosion

Corrosion is a major cause of marine structural accidents. Corrosion results in loss of structural strength at local and global levels, and leads to fatigue failure and stress corrosion cracking. Statistics show that 90% of ship failures were attributed to corrosion [12][13], as shown in Figure 3. Localized corrosion is often found on ship structures. On December 12, 1999, due to severe weather conditions, the Maltese-registered vessel named Erika split into two parts at a sea approximately 70 kilometers off the coast of Brittany, France. At the time of the incident, the vessel was transporting around 30,000 tons of heavy fuel oil, and roughly 19,800 tons were discharged into the sea. This particular oil spill equaled the cumulative volume of oil spilled globally in 1998. The catastrophic incident was a result of a corrosion issue that seemingly persisted on the Erika since 1994 [14].
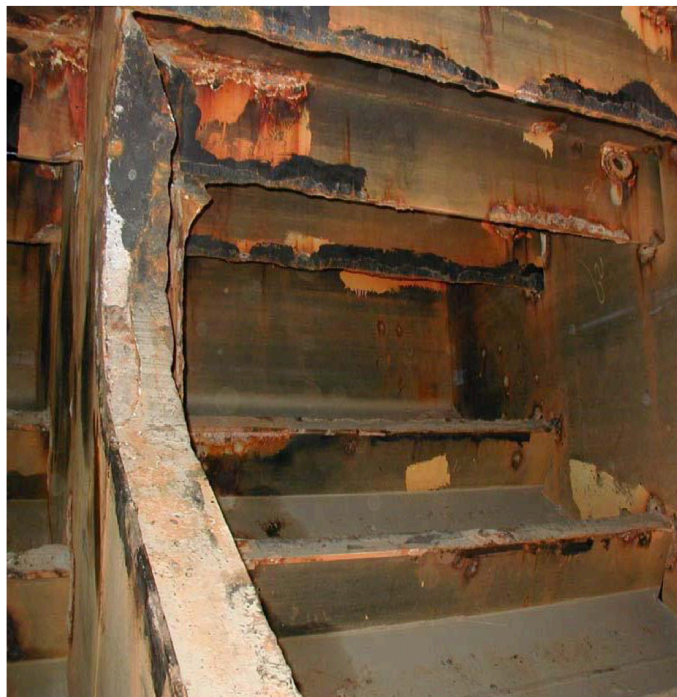
Figure 3. Corroded ballast tank [15].

To cite another example, a floating dry dock with a capacity of 53,400 metric tons was used to dock a Military Sea Lift Command (MSC) class vessel, which had a weight of approximately 42,000 metric tons during docking. Prior to the dry-docking, calculations were conducted to determine the vessel's maximum load per meter, which was found to be 199.0 metric tons per meter. This load was below the dry dock's rated capacity of 206.7 metric tons per meter.The vessel was brought into the dock, and the dock was appropriately de-ballasted to account for the calculated loads. However, upon inspection, it was observed that the pontoon deck exhibited localized buckling. An investigation into the incident revealed that the pontoon deck had suffered significant metal thickness loss due to corrosion. Ultrasonic thickness measurements of the plate indicated that the original metal thickness had been reduced by 18 to 43 percent [16] because of the corrosion.

In another incident, a liberian oil tanker named ABT Summer, which was constructed in South Korea, experienced an explosion off the coast of Angola during its journey to Rotterdam, Netherlands. An explosion on the ship ignited a fire, leading to the complete discharge of its cargo into South Atlantic Ocean. This explosion was reportedly triggered by a corroded ballast tank. The tanker remained ablaze for a period of three days before ultimately sinking, resulting in an oil spill that covered an area of 80 square miles [17].

The ballast tanks of a floating dock are particularly prone to corrosion because they remain in constant contact with seawater, experience high humidity, and are exposed to a chloride-rich environment, even when these tanks are empty [18]. The expenses associated with corrosion are substantial, with a DNV-GL report indicating that the overall cost related to corrosion in European regions exceeds 500 billion Euros, which is approximately 3.8% of the European GDP [19]. In the history of the United States economy, the annual cost of corrosion in 1998 totaled $275.7 billion [20]. These economic losses were provoked by production interruptions, incidents and repairs. The United States marine shipping sector faces yearly expenses of approximately $2.7 billion linked to corrosion. These expenditures are attributed to various categories, including new construction, which accounts for about $1.12 billion, maintenance and repairs, with approximately $810 million, and downtime resulting from corrosion, totaling around $785 million [20], [21]. Frequent repairs and maintenance due to corrosion-related problems lead to operational downtime, resulting in financial losses and impacting maritime schedules and efficiency. Maintenance and repair activities associated with corrosion generate waste, emissions, and environmental hazards, contributing to the environmental impact of maritime operations. The costs linked to corrosion-related maintenance and repairs can substantially escalate, straining budgets and diverting resources from other critical maritime tasks.

Prediction of corrosion rates for the structures and plating are difficult. Some areas of ballast tanks are more prone to corrosion than others according to DNV [22]. In general, areas that are most difficult to protect with coatings (e.g., welds, edges, and details with difficult access) will be the first to be exposed to corrosive ballast water due to early coating breakdown, which can frequently be traced back to substandard treatment of steel surfaces and edges. Accelerated corrosion can occur on these anodic areas due to galvanic effect from large cathodic surfaces with intact coating. Such corrosion is commonly an operational problem, causing much trouble for the owner, sometimes with severe cost implications [23].

The persistent problem of corrosion within ballast tanks presents substantial hazards and inefficiencies in the maritime sector. Ballast tanks are constantly exposed to the harsh marine environment, resulting in the gradual corrosion of their structural components. This corrosion manifests as the deterioration of tank walls, coatings, and essential structural elements, endangering the overall strength of the floating dock. Corrosion undermines the structural components of ballast tanks, heightening the risk of structural failures, leaks, and potential catastrophic incidents. The structural problems caused by corrosion in ballast tanks put the safety of personnel at risk, especially those working in the confined spaces of floating docks, endangering their well-being.

The corrosion in ballast tanks is one of the special risks of the floating docks. The corrosion may also lead to the failures of the pumps, pipes or valves in the ballast system. Therefore, the corrosion is a hybrid risk for the floating docks.

Table 1. Floating dock accident summary

Year	Floating dock	Shipyard	Location	Ship on deck	Reason
2017	Floating dock No. 1 [24]	NAUTA	Gdynia, Poland	"Hordafor V" tanker ship	Stability loss
2018	Floating dock SSR-1 [25]	Morska Stocznia Remontowa Gryfia	Szczecin, Poland	None	Ballast system failure
2018	A floating dock[26]	Hirtshals	Denmark	Hardhaus	Stability loss
2018	Floating dock No. 169 [27]	Slavyanka Port	Primorye Russia	A tanker and a trawler	Not yet defined
2019	Floating dock [8]	Tuzla Ship Repair Yard	Tuzla, Turkey	Asphalt Tanker and an unidentified dry cargo ship.	Overloading
2018	PD -50 Dock [28]	Shipyard No. 82	Roslyakovo, Russia	Russian aircraft carrier	Power outrage of the ballast pumps
2012	Dry Dock #3 [29]	Vigor Industrial Shipyard	Washington	Invader	Valve malfunction
2022	Tsakos floating dock [30]	Montevideo	Montevideo	None	Not yet defined

1.3   Objectives

While there's considerable research on corrosion mitigation in the maritime industry, the distinctive challenges presented by ballast tanks in floating docks demand specialized focus and solutions. This issue becomes urgent due to its direct impact on personnel safety and the environment. Corrosion-related incidents in ballast tanks call for immediate attention and innovative solutions to mitigate risks and environmental harm. The smooth running of maritime activities relies on floating docks working safely and without interruptions. Corrosion causes delays and maintenance issues that get in the way.

To migrate the corrosion risk, this thesis seeks to assess the dynamic behaviours of floating docks with corrosion-induced holes at ballast tanks, with the goal of offering significant insights for the maritime sector on the maintenance approaches required to guarantee the safety of these structures. This study aims to answer how the corrosion-induced holes affect the static and dynamic responses of the floating dock at its working position or during the ballasting and de-ballasting operations.

1.4   Scope of work

According to the abovementioned research motivations, the static and dynamic behaviours of the floating dock are assessed using a numerical method made possible by the help of an in house code which is generated using MATLAB. The safety of the floating dock with corrosion-induced holes is evaluated based on the analyses of the static and dynamic responses. The thesis's contents are organised as follows:

- **Chapter 1:** This chapter explores what led to the thesis, including its background, main motivations and the literature review. It also covers what the project aims to achieve, its scope, and how it's organized.
- **Chapter 2:** This chapter elaborates on the thesis's fundamental theories including the Archimede's principle,equation of motion, strip theory for the hydrostatic force calculations, and the PID controller.

- **Chapter 3:** In this chapter, the research methodology is described. The specifications of the investigated floating dock is given. The adopted models of the six-degree-of-freedom (6-DOF) model, the hydrostatic force model, the hydrodynamic force model, the hydraulic model for the ballast water system and a modified P-controller are elaborated.

- **Chapters 4, 5 and 6:** The results of the dynamic responses of the floating dock during the corrosion-induced ballasting, the automatic ballasting with corrosion-induced holes and the automatic de-ballasting with corrosion-induced holes are discussed. The effects of the corrosion-induced holes on the static and dynamic behaviours of the floating dock are assessed.

- **Chapter 7:** This chapter contains a summary of the thesis. The major conclusions and possibility for further work are discussed in this section.

2 Theory

2.1 Archimede's principle

Archimedes' principle states that when an object is submerged in a fluid, it encounters an upward force equal to the weight of the fluid it displaces. This principle is crucial in understanding the stability of an object floating in still water. The upward buoyancy force is termed as the buoyancy force and is expressed mathematically below.

$$F_B = \rho V g \tag{1}$$

Where, ρ is the density of the fluid, V is the volume of the displaced fluid and g is the acceleration due to gravity, approximately 9.81 m/s² on Earth.

When an object is floating freely in calm water, it experiences a downward force due to gravity, which is typically represented as mg (the weight, where m is the mass and g is the acceleration due to gravity). Because the object remains in equilibrium as shown in Figure 4, there must be an opposing force of the same magnitude and acting in the same direction as the weight to prevent the object from moving. This opposing force is created by the hydrostatic pressures exerted on the object.
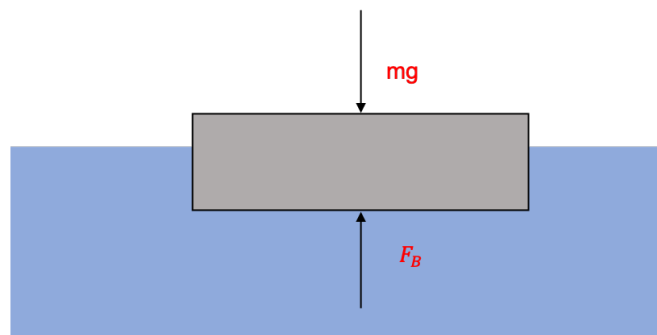
Figure 4. Illustration of the Achimedis principle.

The Archimedes' principle is importance for the static analysis of the marine structures. It can be applied to all structures together with strip theory as described in Section 2.3

2.2 Equation of motion

A structure can move in all six degrees of freedom—surge, sway, heave, roll, pitch, and yaw—if it is free floating or supported by soft mooring lines. The dynamic equations of equilibrium, or equations of motion, can be computed in the frequency domain to ascertain the motion of the structure in each of the aforementioned degrees of freedom.

Newton's second law of motion dictates that a mass system (*M*) will accelerate in the direction of the net force when the vector sum of all forces acting upon it is non-zero [31]. Since the added mass and damping matrices are 6x6. If the off-diagonal elements of the matrix are non-zero, motions in different directions can become coupled. Nonetheless, this coupling is frequently weak. Three terms including the inertia, damping, and restoring force, are associated with the structure in the equations of motion. They are compared to the excitation force exerted on the structure[32].

The equations of motion for six degrees of freedom (k = 6) for a freely floating object is as follows [31]:

$$\sum_{k=1}^{6}\left\{\left[M + A_{jk}\right]\ddot{\eta}_k(t) + B_{jk}\dot{\eta}_k(t) + C_{jk}\,\eta_k(t)\right\} = q_j, \text{ for j} = 1, \dots, 6 \tag{2}$$

Where *M* is the body mass matrix of the system, A_{jk} is the additional mass in mode (j) resulting from motion in mode (k), $\ddot{\eta}_k$ is the structural acceleration in mode (k), $\dot{\eta}_k$ is the velocity vector term, η_k is the displacement vector, B_{jk} represents the frequency dependent potential damping matrix, C_{jk} represents the the hydrostatic stiffness matrix and q_j which is the excitation force .

2.2.1 Mass

The mass term in the equations of motion characterises the system's inertial forces. Typically, this term refers to a mass matrix that distributes the body's mass under study for all degrees of freedom that are taken into account. In the matrix, the rotational degrees of freedom are represented as mass moments of inertia. The forces produced by the body's interaction with the water are also included in this matrix. To model these forces, one can increase the mass in the mass matrix [33]

2.2.2 Added mass

In situations where bodies move erratically underwater or where there is erratic flow around objects, we need to account for the extra effect (force) that the fluid exerts on the structure when computing the equations of motion. This new effect is termed as added mass [34]. The forces produced by additional mass can be computed using strip theory. Using this method, the body under study is divided into multiple smaller "strips" along the main axis. Using tabular values, the added mass for each strip is calculated and then multiplied by the strip's length. Ultimately, the total added mass is calculated by adding all of the strips together.

Figure 5 presents the added-mass coefficients for various two-dimensional shapes like the square, crossed flat plates, finned circle, ellipse, and circle. These shapes exhibit symmetrical properties resulting in residual added-mass coefficients being zero. Consequently, in these instances, there exists no interconnection between the three primary modes of motion for the body. The results depicted in Figure 5 can be achieved by utilizing appropriate conformal mappings [35]

m_{11}:	$\pi\rho a^2$	$\pi\rho b^2$	0
m_{22}:	$\pi\rho a^2$	$\pi\rho a^2$	$\pi\rho a^2$
m_{66}:	0	$\frac{1}{8}\pi\rho(a^2 - b^2)^2$	$\frac{1}{8}\pi\rho a^4$

m_{11}:	$\pi\rho[a^2 + (b^2 - a^2)^2/b^2]$	$\pi\rho a^2$	$4.754\,\rho a^2$
m_{22}:	$\pi\rho a^2$	$\pi\rho a^2$	$4.754\,\rho a^2$
m_{66}:	$*$	$\frac{2}{\pi}\rho a^4$	$0.725\,\rho a^4$
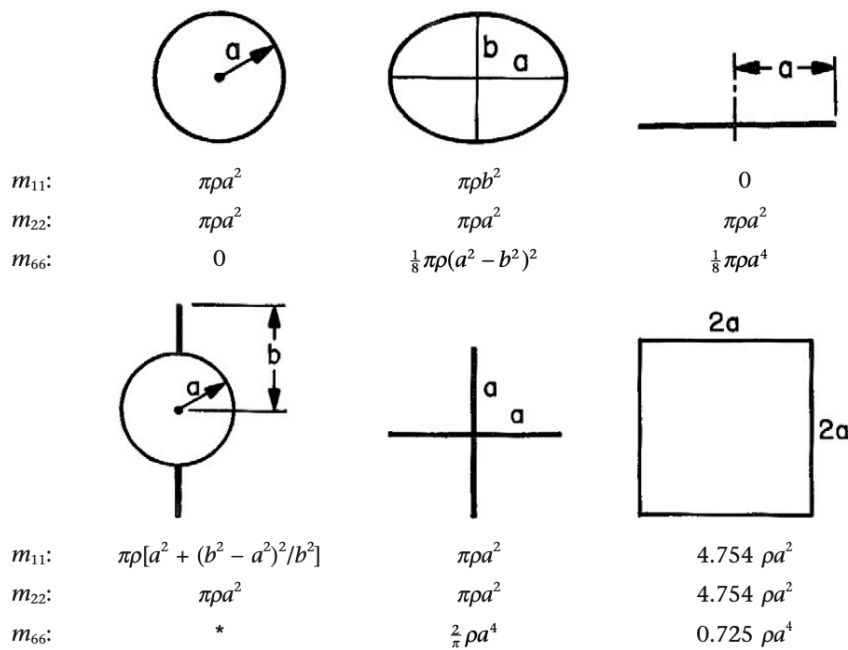
Figure 5. Added-Mass Coefficients for different Two-Dimensional Bodies [35]

2.2.3 Mass moment of inertia

In angular motions, the mass moments of inertia are comparable to mass in translational motion. The difficulty of rotating a body around an axis is determined by its mass moments of inertia [36]. The mass moments of inertia surrounding a barge's origin are the key factor to consider

12

in this situation. In this instance, these moments demonstrate how vulnerable a barge is to roll, pitch, and yaw movements [33]. Usually, the integral calculus is used to determine the mass moments of inertia. The formula below can be used to determine the mass moments of inertia (I) of an element of mass *m* that is situated a distance *r* from the centre of rotation.

$$I = mr^2 \tag{3}$$

where *m* is the body's mass, *R* is the distance between the axis and the rotation mass, and *I* is the mass moment of inertia. Figure 6 shows the mass moment of inertia for various shapes.
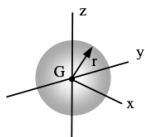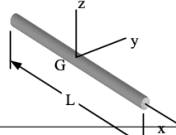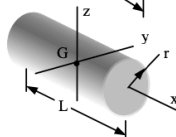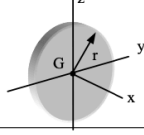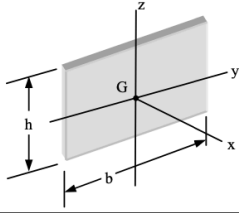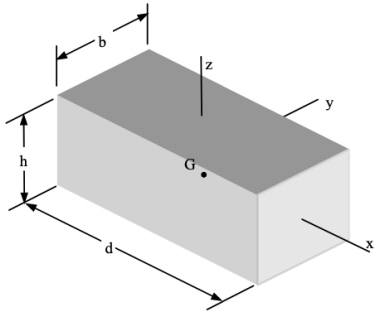
Solid Sphere $I_x = I_y = I_z = \frac{2}{5}mr^2$	
Slender Rod $I_y = I_z = \frac{1}{12}mL^2$	
Solid Circular Cylinder $I_x = \frac{1}{2}mr^2$ $I_y = I_z = \frac{1}{12}m(L^2 + 3r^2)$	
Thin Disk $I_x = \frac{1}{2}mr^2$ $I_y = I_z = \frac{1}{4}mr^2$	
Thin Rectangular Plate $I_x = \frac{1}{12}m(b^2 + h^2)$ $I_y = \frac{1}{12}mh^2$ $I_z = \frac{1}{12}mb^2$	
Brick $I_x = \frac{1}{12}m(b^2 + h^2)$ $I_y = \frac{1}{12}m(h^2 + d^2)$ $I_z = \frac{1}{12}m(b^2 + d^2)$	

Figure 6. Mass moment of inertia for various shapes [37].

2.3 Strip theory

The examination of the movement of vessels is imperitive within the fields of naval architecture and marine engineering. Throughout history, a variety of theories and methodologies have been employed to investigate the performance of ships and other floating structures. Among these theories, one such approach is the hydrodynamic strip theory, which offers a simplified portrayal of the intricate interaction between fluids and structures. This has garnered significant attention due to the time-consuming and costly nature of sea-load experiments and ship motion studies[38]. This theory's essence lies in simplifying a three-dimensional problem by integrating two-dimensional solutions across the length of the ship's cross-sections [39][40].

Hydrodynamic characteristics such as added mass as a result of acceleration, damping as a result of velocity and stiffness which is as a result of the motion component are determined for each individual strip by considering the flow around the two-dimensional sections in Figure 7. The flow around a two-dimensilnal section is transferred into the flow around a uniform cylinder using the Lewis-form method, the Tasai-Porter close-fit mapping method or the Frank close-fit source-distribution method. The overall behavior of the entire structure can be derived by consolidating the results obtained from each individual strip.
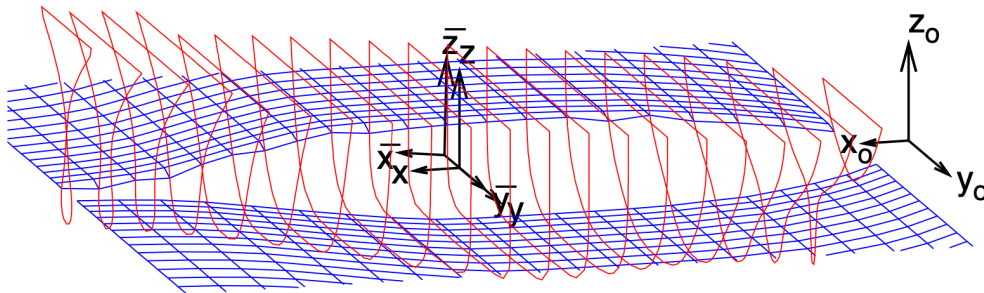
Figure 7 Vessel discretization using strip theory [41].

The first strip theory was established by Korvin-Kroukovsky and Jacob in 1957 for the heave and pitch motions in head waves, and was marked as the pioneering approach. It was well-suited for numerical calculations, and can provide sufficient precision for addressing engineering issues [38].

Subsequent examination of this theory revealed mathematical inconsistencies, especially regarding the coefficients within the equations of motion. The discrepancies primarily originated

from the forward-speed terms , which deviated from the symmetry relationship established by Timman-Newman [42] [43] for the added mass and damping.

In recent years, various modified versions have emerged, with the one formulated by Salvesen, Tuck, and Faltinsen standing out as the most extensively adopted in ship design. This particular version offers reliable performance in predicting the motions of traditional ships and is favored for its computational ease [44]. The concept posits that the vessel possesses a narrow hull shape characterized by symmetrical sides[45]. It moves forward at a steady average speed U within sinusoidal waves, regardless of its orientation. Its movements in the x, y, and z axes are represented as η_1 (surge), η_2 (sway), and η_3 (heave) for translational displacements. Additionally, rotational motions around the x, y, and z axes are denoted by η_4 (roll), η_5 (pitch), and η_6 (yaw) correspondingly, as depicted in Figure 8.

We assume that responses are harmonic and linear. Since the viscous effects are ignored, the fluid motions can be taken to be irrotational, and the potential flow theory can be used to construct the problem [46]. The velocity potential for an incident wave is:

$$\Phi_0(x, y, z; t) = \Phi_0(x, y, z)e^{-iw_e t} \tag{4}$$

Here, w_e represents the encounter frequency, which is associated to the wave frequency ω by:

$$w = w_e + kU cos\beta \tag{5}$$

Where β is heading angle and k is the wave number.
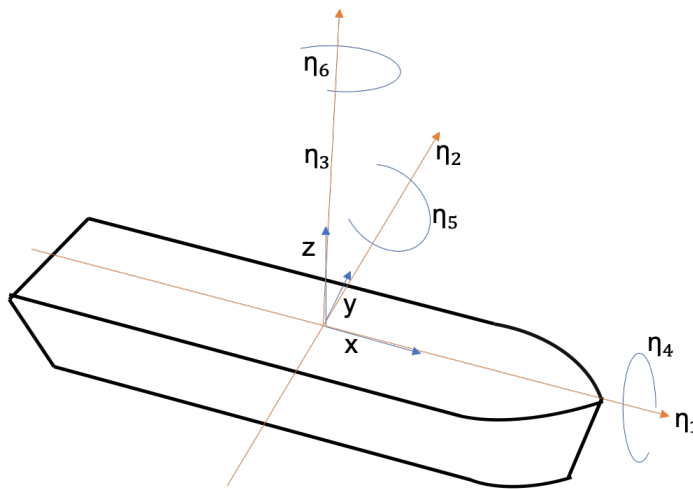
Figure 8. Description of the ship motions.

The distinctions between the treated approaches begin at this stage, where the complex amplitude of the incident wave potential can be described in terms of real and imaginary. Another limitation aside from the one listed above is that strip theories can reliably forecast ship movements even when the length-to-beam ratios are as small as 2.5 [47].

2.4 PID Controller

The acronym PID stands for proportional integral derivative, a control algorithm utilized in industrial settings to manage various process variables such as pressure, flow, temperature, and speed. This controller employs a feedback mechanism within a control loop to regulate these variables effectively. This type of control is pivotal for guiding a system toward a particular desired point or level. It's extensively used in temperature regulation, various scientific processes, automation, and numerous chemical applications. Operating on closed-loop feedback, this controller aims to closely match the actual output with the desired output or a predetermined fixed point whenever possible [48].

The PID controller employs three fundamental control behaviors to minimize the error between the process variable and the desired setpoint through closed-loop operations.

1. Proportional (P): This behavior adjusts the output proportionally to the current error. The larger the error, the larger the corrective effort applied by the controller. However, this action alone can lead to a steady-state error.

2. Integral (I): The integral action considers the accumulation of past errors over time and applies corrective action based on this accumulated error. It helps eliminate any residual steady-state error by continuously integrating the error and adjusting the output accordingly.

3. Derivative (D): This behavior looks at the rate of change of the error over time. It anticipates future error trends and acts to counteract rapid changes, thus damping oscillations and improving system stability.

The diagram below illustrates the setup of a PID controller, comprising a PID block transmitting its output to the process block. The process, encompassing final control instruments such as actuators and valves, manages diverse industrial operations. The PID algorithm receives an error signal, e(t), which is produced when the process's output is compared to a reference signal, u(t). Through the use of the algorithm's derivative, integral, and proportional control

calculations, the controller produces a combined response or controlled output that is applied to the plant's control devices.
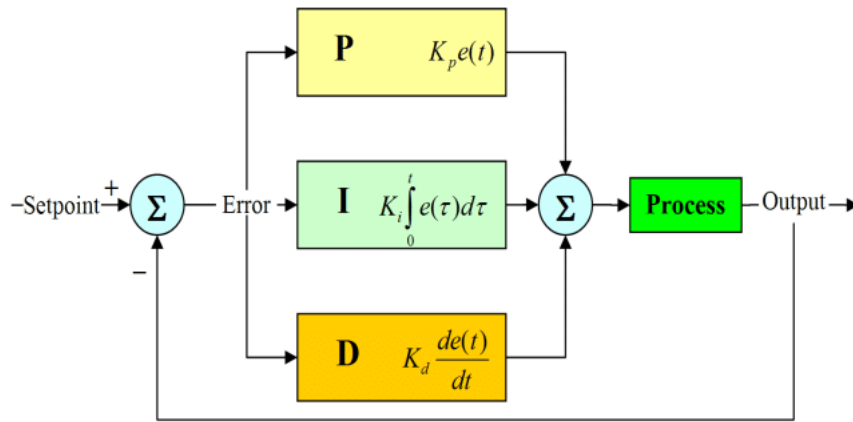
Figure 9 PID block diagram [49]

Not all control scenarios necessitate all three control elements. Frequently, practical applications employ combinations like PI and PD controls.

The final out of the PID is based on the equation below;

$$U(t) = K_p * e(t) + K_i \int_0^t e(t) + K_d \frac{de(t)}{dt} \qquad (6)$$

Whereas, $U(t)$ is the PID output, K_p is the Proportional gain, $e(t)$ is the error at time t, K_i is the integral gain and lastly K_d is the derivative gain .

3 Methodology

3.1 Specifications of the floating dock system

The floating dock arrangement comprises a dock, a vessel, mooring ropes connecting them, and mooring lines fastened to the dock and the docking blocks on the pontoon deck, as illustrated in Figure 10. Table 2 details the specifications of this floating dock system, including the initial center of gravity (CoG) for both the dock and the vessel. These measurements are explained within a global coordinate system termed OXYZ, with its origin positioned at the center of the dock's keel. The X-axis indicates the direction along the keel, from the aft to the fore side. The Y-axis signifies the side-to-side direction, while the Z-axis extends vertically upward from the dock's bottom. As the dock moves, a body-fixed coordinate system referred to as OXYZ gradually differs from the global coordinate system. The mass moments of inertia listed in Table 2 are specific to the body-fixed coordinate system, but the mass moments of inertia is about the CoG.
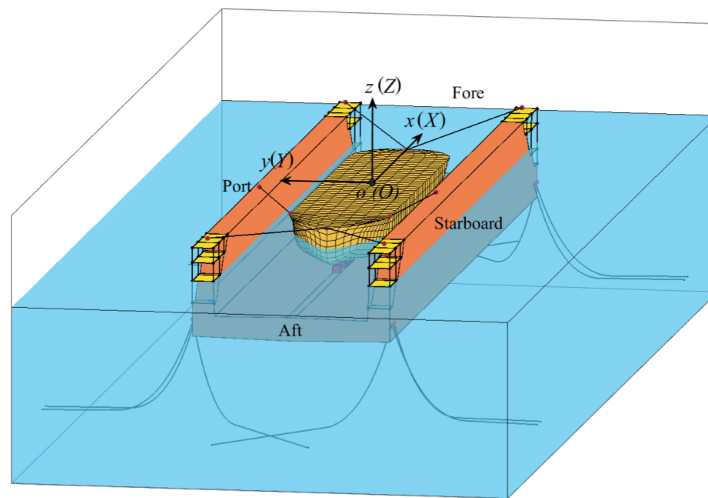
Figure 10 Illustration of a floating dock system.

An initially aligned oxyz coordinate system, fixed to the body, aligns with the global coordinate system. As the floating dock moves, this body-fixed coordinate system shifts away from the global one. Table 2 presents specifications for the floating dock system, while Figure 11 details the ballast tanks, specifying their number and maximum volume.

PORT SIDE

Volume of tank 1 (1965 m^3)	Volume of tank 2 (2144 m^3)	Volume of tank 3 (2110 m^3)	Volume of tank 4 (2145 m^3)	Volume of tank 5 (2145 m^3)	Volume of tank 6 (1856 m^3)
Volume of tank 7 (1653 m^3)	Volume of tank 8 (1837 m^3)	Volume of tank 9 (1837 m^3)	Volume of tank 10 (1837 m^3)	Volume of tank 11 (1837 m^3)	Volume of tank 12 (1653 m^3)
Volume of tank 13 (2093 m^3)	Volume of tank 14 (2267 m^3)	Volume of tank 15 (2267 m^3)	Volume of tank 16 (2267 m^3)	Volume of tank 17 (2267 m^3)	Volume of tank 18 (1978 m^3)

AFT — FORE

STARBOARD

Figure 11 Details of the ballast tanks.

Table 2 Specifications of the floating dock system.

Dimension of dock $L_d \times B_d \times H_d$	$\mathbf{168.48\ m \times 39.8\ m \times 18.2\ m}$
Mass of dock	5.1782×10^6 kg
Initial X of the dock's CoG	-0.435 m
Initial Y of the dock's CoG	0.093 m
Initial Z of the dock's CoG	5.497 m
Dock's mass moment of inertia I_{11dock}	9.56×10^8 kg·m^2
Dock's mass moment of inertia I_{22dock}	1.026×10^{10} kg·m^2
Dock's mass moment of inertia I_{33dock}	1.096×10^{10} kg·m^2
Dimension of vessel $L_v \times B_v \times H_v$	$95.217\ m \times 20\ m \times 8\ m$
Mass of vessel	5.1292×10^6 kg
Initial X of the vessel's CoG	-0.435 m
Initial Y of the vessel's CoG	0.093 m
Initial Z of the vessel's CoG	13.09 m
Vessel's mass moment of inertia $I_{11vessel}$	2.234×10^8 kg·m^2
Vessel's mass moment of inertia $I_{22vessel}$	2.968×10^9 kg·m^2
Vessel's mass moment of inertia $I_{33vessel}$	2.968×10^9 kg·m^2
Density of seawater	1025 kg/m^3
Gravitational acceleration	9.81 m/s^2

3.2 6-DOF model

The movements of the floating dock are updated utilizing a 6-degree-of-freedom (6-DOF) model. This model encompasses both the dock's linear movement equations within the overall

coordinate system and the dock's rotational movement equations articulated within the body-fixed coordinate system. The equations governing the linear movements are presented in Equation 3, derived from Newton's Second Law.

$$\frac{D^2 X_{CG}}{dt^2} = m^{-1} \sum F_G \tag{7}$$

where $\mathbf{X}_{CG} = (X_{CG}, Y_{CG}, Z_{CG})$ represents the CoG of the floating dock, $\boldsymbol{m}$ represents the mass matrix of the floating dock. $\boldsymbol{F}_G$ is denoted as the external force vector applied to the CoG. The dock's angular velocity vector is modelled using Eq.(8) [50].

$$\frac{D\omega_B}{dt} = I^{-1} \left[\sum M_B - \omega_B \times (I\omega_B) \right] \tag{8}$$

where $\boldsymbol{I}$ represents the inertial tensor of the floating dock, $\boldsymbol{M}_B$ is the moment vector and $\boldsymbol{\omega}_B = (\omega_{B1}, \omega_{B2}, \omega_{B3})$ is the dock's angular velocity vector. The rotational angles of the floating dock are computed using Eq.(9).

$$\begin{aligned} \frac{D\phi}{dt} &= (\omega_{B2}\sin\gamma + \omega_{B3}\cos\gamma)/\cos\psi \\ \frac{d\psi}{dt} &= (\omega_{B2}\cos\gamma - \omega_{B3}\sin\gamma) \\ \frac{d\gamma}{dt} &= \omega_{B1} + (\omega_{B2}\sin\gamma + \omega_{B3}\cos\gamma)\tan\psi \end{aligned} \tag{9}$$

The yaw pitch and roll angles are denoted as ϕ, ψ and γ are the yaw, respectively. The position of a point on the dock or vessel in the global coordinate system can be obtained from its position in the body-fixed coordinate systems using Eq. (10) based on the coordinate transformations of rotation axes.

$$\begin{bmatrix} X - X_{CG} \\ Y - Y_{CG} \\ Z - Z_{CG} \end{bmatrix} = \begin{bmatrix} \cos\phi & -\sin\phi & 0 \\ \sin\phi & \cos\phi & 0 \\ 0 & 0 & 1 \end{bmatrix} \begin{bmatrix} \cos\psi & 0 & \sin\psi \\ 0 & 1 & 0 \\ -\sin\psi & 0 & \cos\psi \end{bmatrix} \begin{bmatrix} 1 & 0 & 0 \\ 0 & \cos\gamma & -\sin\gamma \\ 0 & \sin\gamma & \cos\gamma \end{bmatrix} \begin{bmatrix} x - x_{CG} \\ y - y_{CG} \\ z - z_{CG} \end{bmatrix} \tag{10}$$

In the current 6-DOF model, the way the dock and vessel interact is approximated. Initially, the model updates the dock's movements considering its mass, mass moments of inertia, and the external forces affecting it, before the vessel makes contact with the blocks on the pontoon deck. Once the vessel touches these blocks, both the dock and vessel are treated as a unified rigid body, having a combination of mass and mass moments of inertia. An estimated contact force between the dock and vessel is determined as the disparity between the vessel's gravity force and its buoyancy. This calculated force is employed to verify if contact between the vessel and dock occurs.

3.3 Hydrostatic force model

The buoyancy forces acting on the dock and vessel, along with the gravitational forces exerted by the water in the ballast tanks, are collectively referred to as hydrostatic forces. These forces are determined through calculations based on Archimedes' principle. To determine the submerged volumes of the floating dock and ballast tanks, a strip theory is applied. This theory involves breaking down the three-dimensional (3D) structure into two-dimensional (2D) sections for assessment.

The total hydrostatic loads on the 3' structure are determined by integrating the hydrostatic forces longitudinally along the floating dock and ballast tanks. The submerged areas of the 2D sections are defined by a set of boundary points, allowing for the calculation of their area, first moment of area, and second moment of area. These parameters for the submerged sections are detailed in Table 3.

Using the section areas, the displaced water volume of the dock and vessel, as well as the volume of ballast water, can be computed by integrating along the longitudinal direction. S_y and S_z are used to calculate the centroid of the submerged region as $y_0 = S_z/A$ and $z_0 = S_y/A$. I_y and I_z are used to calculate the mass moment of inertia of the ballast water in Eq. (8). The surface integrals are transferred to line integrals. The boundaries of the line integrals for the immersed region are discretized as N number of points (y_k, z_k). In Table 4, $\bar{y}_{1,k} = 0.5(y_k + y_{k+1})$, $\bar{z}_{1,k} = 0.5(z_k + z_{k+1})$, $\bar{y}_{2,k} = 0.5(y_k^2 + y_{k+1}^2)$, $\bar{z}_{2,k} = 0.5(z_k^2 + z_{k+1}^2)$, $\bar{y}_{3,k} = 0.5[(y_k - y_{CG})^2 + (y_{k+1} - y_{CG})^2]$, $\bar{z}_{3,k} = 0.5[(z_k - z_{CG})^2 + (z_{k+1} - z_{CG})^2]$, $\Delta y_k = y_{k+1} - y_k$ and $\Delta z_k = z_{k+1} - z_k$. The centroid of the submerged area is calculated as $y_0 = S_z/A$ and $z_0 = S_y/A$.

Table 3 Area, first moments and second moments of area for the submerged sections.

Variables	Surface integral	Discretization
A	$\iint dydz$	$\sum_{k=1}^{N} -\bar{z}_{1,k}\,\Delta y_k$
S_y	$\iint zdydz$	$-\dfrac{1}{6}\sum_{k=1}^{N}(2\bar{z}_{1,k}^2 + \bar{z}_{2,k})\,\Delta y_k$
S_z	$\iint ydydz$	$\dfrac{1}{6}\sum_{k=1}^{N}(2\bar{y}_{1,k}^2 + \bar{y}_{2,k})\,\Delta z_k$
I_y	$\iint (z - z_{CG})^2 dydz$	$-\dfrac{1}{3}\sum_{k=1}^{N}(\bar{z}_{1,k} - z_{CG})\,\bar{z}_{3,k}\Delta y_k$
I_z	$\iint (y - y_{CG})^2 dydz$	$\dfrac{1}{3}\sum_{k=1}^{N}(\bar{y}_{1,k} - y_{CG})\,\bar{y}_{3,k}\Delta z_k$

It should be noted that the immersed region of the body is determined based on the dock's draught, the heel and trim angles. The dock's draft, the heel and trim angles and the sea water level are known when calculating the dock's hydrostatic loads. However, the height of the water level in a ballast tank is unknown. It can be calculated using a secant iteration method of a single point. After the ballast water volume in a tank is updated, the water level can be obtained using Eq. (11)

$$h^{(n+1)} = h^{(n)} - \frac{h^{(n)} - h_{\text{pre}}}{V^{(n)} - V_{\text{pre}}}(V^{(n)} - V) \tag{11}$$

where V is the given water volume in a ballast tank, h_{pre} is the height of the water level in the previous time step and V_{pre} is the water volume for the water level h_{pre}.

3.4 Hydrodynamic force model

The hydrodynamic force model is proposed to address the effects of added mass and dynamic damping of the floating dock and the docked vessel. For the added mass effect, only the

added mass and mass moments of the dock are considered, while those of the vessel are neglected. For the dynamic damping effect, the damping coefficients are calculated in different ways before and after the vessel contacts the blocks.

An added mass model based on the added mass and mass moments of inertia of 2D plate is proposed. The 3D results are formed by integrating the 2D results along the longitudinal direction of the dock. The 3D correction given by the aspect-ratio formula of Pabst [51]

$$\Psi(B/L) = \frac{1}{\sqrt{1 + (B/L)^2}}\left(1 - \frac{0.425B/L}{1 + (B/L)^2}\right) \tag{12}$$

Table 4 shows the formulas and results of the floating dock's added mass and mass moment of inertia. The components of surge, sway and yaw are neglected in the present model because they are small compared with the heave, roll and pitch components.

Table 4 Formulas and results of added mass and mass moment of inertia.

Motion	Formula	value
Heave	$m_{33added} = \frac{1}{8}\rho\pi B^2 L\Psi(B/L)$	9.4604×10^7 kg
Roll	$I_{11added} = \frac{1}{256}\rho\pi B^4 L\Psi(B/L)$	4.6830×10^9 kg $\cdot$ m^2
Pitch	$I_{22added} = \frac{1}{96}\rho\pi B^2 L^3\Psi(B/L)$	2.2378×10^{11} kg $\cdot$ m^2

In the dynamic damping model, the damping coefficients are calculated using the mass matrices of the dock (vessel), a damping ratio of 5% and natural frequencies of the heave, roll and pitch motions of the dock. The natural frequencies are calculated using Eq. (13) [52].

$$\omega_{heave} = \sqrt{\frac{C_{33}}{m_{33}}}, \quad \omega_{roll} = \sqrt{\frac{C_{44}}{I_{11}}}, \quad \omega_{pitch} = \sqrt{\frac{C_{55}}{I_{22}}} \tag{13}$$

where m_{33}, I_{11} and I_{22} include the contributions of the dock, ballast water and dock's added mass, and C_{33}, C_{44} and C_{55} are the hydrostatic restoring coefficients in heave, roll and pitch motions, respectively. Figure 12 illustrates the hydrostatic restoring coefficients in heave, roll and pitch

motions of the dock-vessel system, which are combination of the coefficients of the dock and the vessel based on the relative positions of the dock and the vessel. When the draught is larger than 6.2m, the waterplane of the vessel is involved and the KB and KG of the dock-vessel system are adopted.
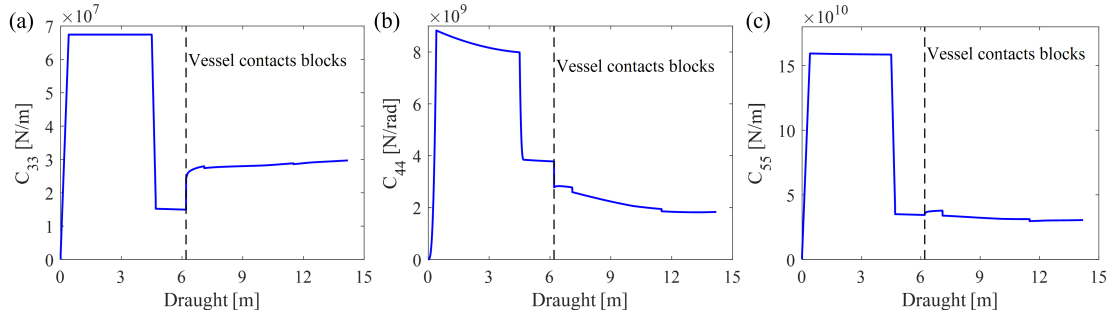
Figure 12 Hydrostatic restoring coefficients in heave, roll and pitch motions of the dock-vessel system [53].

3.5 Hydraulic model of the ballast water system

The floating dock incorporates six ballast pumps, each overseeing three ballast tanks arranged from port to starboard, as illustrated in Figure 13. Pipes linked to these tanks have a diameter of 400mm, while the primary pipe boasts a larger diameter of 600mm. Every ballast tank is outfitted with its own butterfly valve, and the primary pipes contain inlet and outlet valves utilized for ballasting and de-ballasting activities, respectively. Furthermore, a connecting pipe, measuring 400mm in diameter, accompanied by a corresponding connection valve, allows the pipe network to interface with other pumps.
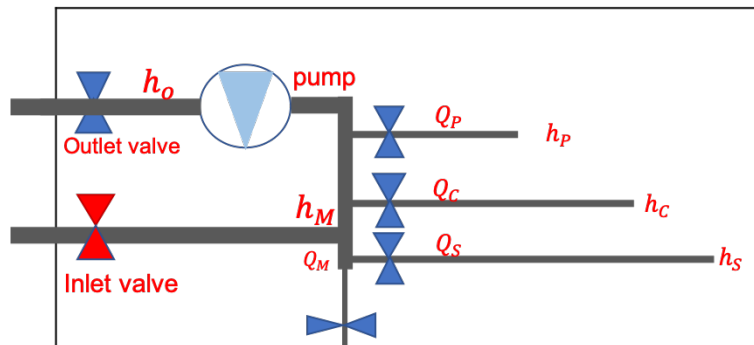
Figure 13 Schematic of the ballast water system during the de-ballasting operation.

During the de-ballasting operation shown in Figure 13, the valves at port, center, and starboard, as well as the outlet valve, are open, facilitating the discharge of water from the tanks. Meanwhile, both the inlet valve and connection valve remain closed. Conversely, in the ballasting process, the inlet valves are opened to enable water entry into the tanks, while the outlet valves stay closed. The positions of the other valves remain unchanged in comparison to the de-ballasting operation.

The hydraulic calculations of the ballast water system are based on the pressure changes of different elements, i.e., pipe, valve and pump. The changes of water heads, representing the pressure drops along the pipes are neglected and those of the valves and pumps are considered. The changes of water heads at outlet, port, centre and starboard valves are calculated as:

$$h_O - h_{out} = \lambda_M |Q_M| Q_M \tag{14}$$
$$h_P - h_M = \lambda_P |Q_P| Q_P \tag{15}$$
$$h_C - h_M = \lambda_C |Q_C| Q_C \tag{16}$$
$$h_S - h_M = \lambda_S |Q_S| Q_S \tag{17}$$

where h_M, h_P, h_C, h_S, and h_O are the water heads at right sides of pump, port, centre, starboard and outlet (inlet) valves in Figure 13, and h_{out} is the water head at the left side of outlet valve. Q_M, Q_P, Q_C and Q_S are the flow rates in main, port, center and starboard pipes. The coefficients λ_M, λ_P, λ_C and λ_S are given by the KV values of the butterfly valves, as shown in Table 5.

Table 5 KV values of different opening angles for the butterfly valves [54].

θ [º]	20	30	40	50	60	70	80	90
KV of 400 mm	155	475	105	1880	3150	5250	9450	10500
KV of 600 mm	375	1125	2500	4500	7500	12550	22500	25000

The KV value is the volume of water (measured in m^3) that will pass through the valve in one hour at a pressure drop of 1bar. The KV values depend on the valve opening angles and are given by experimental measurements [54]. The expression of λ can be written as Eq. (18)

$$\lambda = \frac{1}{g(KV/36000)^2} \quad [s^2/m^5] \tag{18}$$

The water head of pumps is calculated using Eq. (19).

$$h_O - h_M = h_0 - \lambda_{\text{pump}}|Q_M|Q_M \tag{19}$$

where $h_0 = 21.25\text{m}$ is the pump's total water head with zero flow rate and $\lambda_{\text{pump}} = 20\text{s}^2/\text{m}^5$ is the pump coefficient. The continuity equation between the main pipe and the branch pipes is given by Eq. (20).

$$Q_M = Q_P + Q_C + Q_S \tag{20}$$

For the ballasting operation, the solution is given by taking $h_0 = 0$ and $\lambda_{\text{pump}} = 0$. The flow rate through the hole is then given by Eq.(21).

$$Q = \frac{(h_{out} - h)}{\sqrt{\lambda_{\text{hole}}|h_{out} - h|}} \tag{21}$$

Where h_{out} is the water level outside the ballast tank, λ_{hole} is hole coefficient. λ_{hole} can be calculated using Eq. (18) and the KV values in Table 6.

Table 6 KV values at different hole diameter for the butterfly valves [54].

D [mm]	40	50	65	80	100	125	150	200	250	300	400
KV	53	133	240	410	665	900	1800	3550	7350	9100	10500

After the flow rate of a ballast tanks is obtained, the ballast water volume is updated using Eq. (22)

$$\frac{d\alpha_j}{dt} = \frac{Q_j}{V_{\text{max},j}} \tag{22}$$

where α_j is the volume fraction of the water in j^{th} ballast tank, $V_{\text{max},j}$ is the total volume of jth tank and Q_j is the corresponding flow rate.

3.6 Modified P-controller for the ballast control system

The objective of the ballast control system is to maintain stability during docking operations, specifically by controlling the pitch and roll angles within acceptable limits. The focal points for control are the angles at which the valves are opened, organized into six groups, as depicted in Table 7. The specific valve opening angles for the 18 tanks are provided in Eq. (23).

$$\theta_{\text{target},i}^n = \theta_{max}\min\{1 + K_p^n c_{p,i}L\psi + K_r^n c_{r,i}B\gamma, 1\} \tag{23}$$

$$K_p^{n+1} = \begin{cases} K, & |\psi| > \psi_{upper} \\ 0, & |\psi| < 0.1\psi_{upper}, \\ K_p^n, & \text{otherwise} \end{cases} \qquad K_r^{n+1} = \begin{cases} K, & |\gamma| > \gamma_{upper} \\ 0, & |\gamma| < 0.1\gamma_{upper} \\ K_r^n, & \text{otherwise} \end{cases} \tag{24}$$

K represents the total control coefficient while θ_{max}.denotes the maximum valve opening angle. When the mean sea water level lower than the pontoon deck, θ_{max} is set to 90deg. However, if the mean sea water level is higher, θ_{max} is adjusted to 70deg, as optimized by Wen et al. [54]. Table 7 illustrates the pitch and roll control coefficients for various valve groups involved in the ballasting operation. These coefficients display opposite signs during the de-ballasting operation. In de-ballasting, a minimum valve opening angle of 35deg is maintained to optimize pump efficiency and safeguard the pump's integrity. However, during gravitational ballasting, the minimum valve opening angle is set to be 0deg.

Table 7 Pitch and roll coeffiecients for ballasting operation.

Control group of valves	No.1-3	No.4-6	No.7-9	No.10-12	No.13-15	No.16-18
Pitch control coefficient $c_{p,i}$	-1	1	-1	1	-1	1
Roll control coefficient $c_{r,i}$	-1	-1	0	0	1	1

The relation between the real valve opening angle and the control signal in Eq. (23) is given in Eq. (25) based on the valve mechanics.

$$\theta_{\text{present},i}^{n+1} = \begin{cases} \theta_{\text{present},i}^n + \Delta t\omega_{\text{valve}}, \theta_{\text{present},i}^n < \theta_{\text{target},i}^n - \Delta t\omega_{\text{valve}} \\ \theta_{\text{present},i}^n + \Delta t\omega_{\text{valve}}, \theta_{\text{present},i}^n > \theta_{\text{target},i}^n + \Delta t\omega_{\text{valve}} \\ \theta_{\text{present},i}^n, \text{otherwise} \end{cases} \tag{25}$$

where $\omega_{\text{valve}} = 90\text{deg/min}$ is the angular velocity of the valve and Δt is the time step. The target valve angles will be updated in every duration of $\Delta T = N_T \Delta t$ and based on the conditions in Eqs. (24) − (25). When all these conditions are not satisfied, they are kept the same values with the previous time-step to avoid frequently changing the control signals. A control range is defined as $\Delta D = L\psi_{upper} = B\gamma_{upper}$ to balance the controls in the pitch and roll motions. Based on the studies of Wen et al. [54] the control parameters are listed as $K = 0.5$, $\Delta D = 0.1\text{m}$, $N_T = 5$.

4 Corrosion-induced Ballasting

4.1 Case description

The corrosion-induced ballasting is the ballasting of the floating dock due to the corrosion-induced holes located at the ballast tanks. The floating dock is at its working position with a draught of 3.5m. The automatic ballast control is off because the valves and pumps are not active in this situation. The dock will tilt when there is corrosion-induced holes located at one or two ballast tanks. This present study involve es two scenarios: one is that a corrosion-induced hole with different diameters occurs in one single ballast tank and another is that two ballast tanks have corrosion-induced holes of 300mm each.

The sensitivity study of section number for the dock and the ballast tanks, and the convergence study of the water level in ballast tanks were given in Zhang et al. [56]. Based on the convergent results of the section number for the dock and the ballast tanks, the dock is discretized into 150 sections and each ballast tank is sliced into 20 sections in the present study. The number of points for a dock's section is 18 and those of port, centre and starboard tanks are 8, 8 and 6, respectively.

4.2 Results and discussions

To guarantee the dock's performance under these unexpected circumstances, a time-step sensitivity analysis is initially needed to conduct. Figure 14 shows the time-step sensitivity study of the draught, pitch and roll angles during the corrosion induced accident in Tank No.1, where the hole diameter is 50mm. Three time-steps of 1s, 0.5s, and 0.25s are examined to assess the convergence of the results. The results obtained using these three different time steps appear almost identical. A time step of 0.5s is chosen to proceed the further analysis to achieve a balance between the computational time and the temporal resolution. As can be seen in Figure 14, the draught becomes larger as the weight of the ballast water increases. The dock continues to tilt with final heel and trim angles of 0.55º and 0.14º respectively.
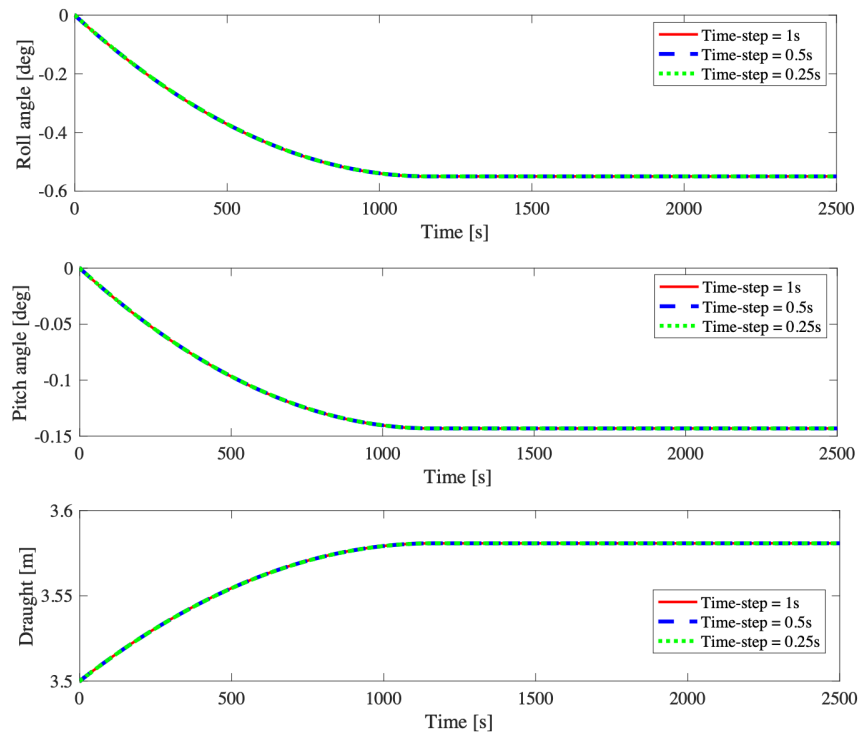
Figure 14 Time-step sensitivity study of the draught, pitch and roll angles during the corrosion induced accident in Tank No. 01, where the hole diameter is 50mm.

Figure 15 shows the roll and pitch angles for the scenarios of one corrosion hole with different diameters located at Tank. No.01. The roll and pitch angles of different hole diameters have the same final convergent results. Table 8 presents the time taken to fill up the ballast tank through the corrosion hole in Tank No. 01. The time is recorded when the flow rate through the hole decreases to $0.5 \times 10^{-3} \mathrm{m}^3/\mathrm{s}$. From the table, the time increases with a decreasing hole diameter. For a hole diameter of 300mm, the dock tilts to the maximum heel and trim in about half an hour.
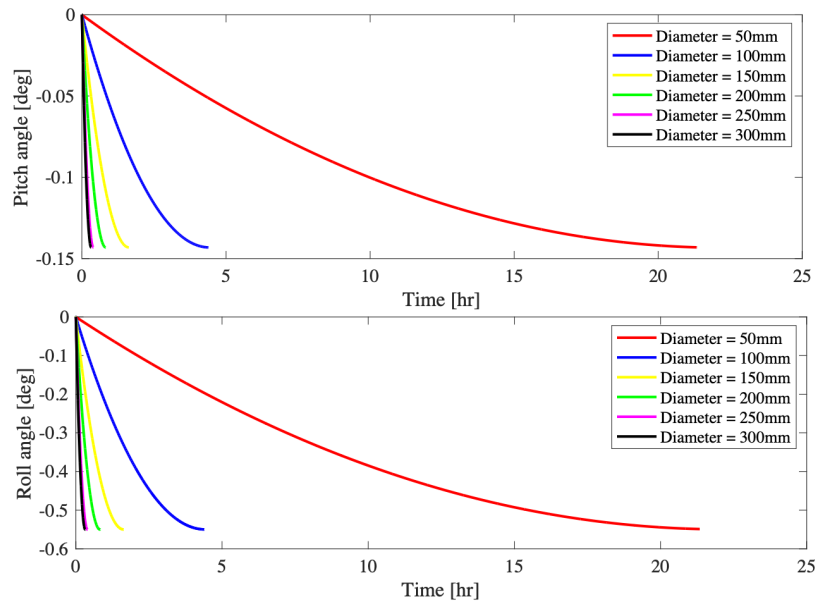
Figure 15 Roll and pitch angles for the scenarios of one corrosion hole with different diameters located at Tank. No.01.

Table 8 Time taken to fill the ballast tank through the corrosion hole in Tank No. 01.

Hole diameter [mm]	Duration time [hour]
50.00	21.34
100.00	4.39
150.00	1.63
200.00	0.83
250.00	0.40
300.00	0.32

Figure 16 shows the maximum pitch and roll angle for the scenarios of one corrosion hole with a diameter of 300mm located at different ballast tanks. A large maximum pitch angle corresponds to the hole located at the tanks near the aft or fore, and a large maximum roll angle corresponds to the hole located at the tanks near the port or starboard. It can be attributed to the moment due to the extra weight of the ballast water flow into the tank through the corrosion hole. The maximum roll angles of the scenarios of one corrosion hole located at the starboard tanks are always larger than those at the port tanks.

The reason is that the total volumes of the starboard tanks are larger than those of the port tanks, as shown in Figure 11. Figure 17 shows the volumes of the ballast water in Tanks No.02 and

tank No.14 for the scenarios of one corrosion hole located at Tanks No.02 and 14, respectively. The volume of the ballast water in Tank No. 14 is much larger than that in Tank No.02, which can also explain the reason of the different maximum roll angle in Figure 16 (b).

0.14	0.09	0.03	0.03	0.09	0.14
0.17	0.11	0.03	0.03	0.11	0.17
0.18	0.12	0.04	0.04	0.11	0.17

a) Maximum pitch angle [°]

0.55	0.58	0.54	0.56	0.58	0.55
0.00	0.00	0.00	0.00	0.00	0.00
0.72	0.75	0.71	0.68	0.71	0.69

b) Maximum roll angle [°]

Figure 16 Maximum pitch and roll angles for the scenarios of one corrosion hole with a diameter of 300mm located at different ballast tanks.
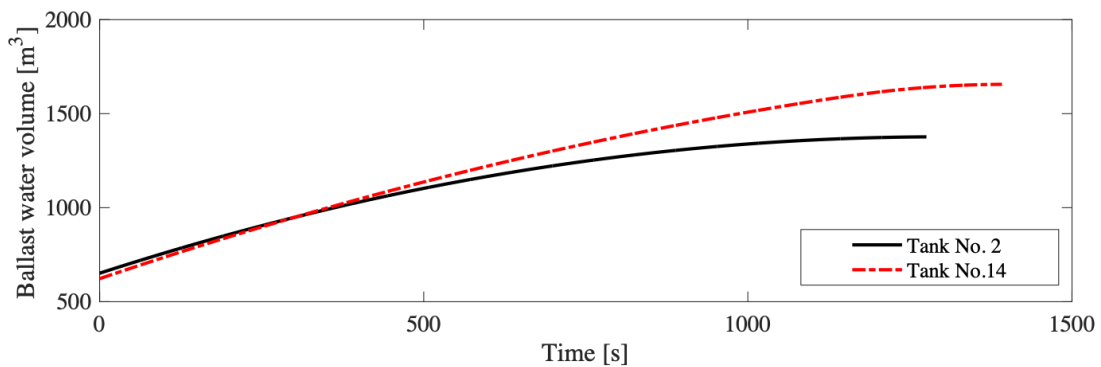
Figure 17 Volume of different tanks after ballasting procedure.

Figures 18 and 19 show the maximum pitch and roll angles for the scenarios of two corrosion holes with a diameter of 300mm located at different ballast tanks. The distributions follow the principle as discussed for one corrosion hole cases.

A large maximum pitch angle corresponds to the holes located at the tanks near the aft or fore, and a large maximum roll angle corresponds to the holes located at the tanks near the port or starboard. The maximum pitch and roll angles for two corrosion hole cases are 0.42º and 2.04º respectively. Also since these maximum pitch and roll angles are achieved at the last time-step, this suggests that the water inside the ballast tanks has reached a stable state. At this point, there would be no further changes in the water level or weight distribution.

tank No.	1	2	3	4	5	6	7	8	9	10	11	12	13	14	15	16	17	18
1	0.14	0.30	0.21	0.13	0.06	0.00	0.35	0.27	0.19	0.12	0.05	0.00	0.31	0.24	0.17	0.11	0.05	0.00
2	0.30	0.09	0.15	0.07	0.00	0.06	0.29	0.21	0.14	0.06	0.00	0.06	0.25	0.19	0.12	0.06	0.00	0.05
3	0.21	0.15	0.03	0.00	0.06	0.12	0.18	0.13	0.06	0.00	0.06	0.11	0.17	0.11	0.06	0.00	0.05	0.10
4	0.13	0.07	0.00	0.03	0.14	0.21	0.12	0.06	0.00	0.06	0.13	0.19	0.11	0.06	0.00	0.06	0.11	0.17
5	0.06	0.00	0.06	0.14	0.09	0.32	0.06	0.00	0.06	0.13	0.21	0.28	0.05	0.00	0.06	0.12	0.19	0.25
6	0.00	0.06	0.12	0.21	0.32	0.14	0.00	0.05	0.12	0.19	0.27	0.35	0.00	0.05	0.11	0.17	0.24	0.31
7	0.35	0.29	0.18	0.12	0.06	0.00	0.17	0.32	0.22	0.14	0.06	0.00	0.42	0.32	0.22	0.13	0.06	0.00
8	0.27	0.21	0.13	0.06	0.00	0.05	0.32	0.11	0.16	0.07	0.00	0.06	0.33	0.24	0.15	0.07	0.00	0.06
9	0.19	0.14	0.06	0.00	0.06	0.12	0.22	0.16	0.03	0.00	0.07	0.13	0.22	0.15	0.07	0.00	0.07	0.13
10	0.12	0.06	0.00	0.06	0.13	0.19	0.14	0.07	0.00	0.03	0.15	0.22	0.13	0.07	0.00	0.07	0.15	0.22
11	0.05	0.00	0.06	0.13	0.21	0.27	0.06	0.00	0.07	0.15	0.11	0.33	0.06	0.00	0.07	0.16	0.24	0.33
12	0.00	0.06	0.11	0.19	0.28	0.35	0.00	0.06	0.13	0.22	0.33	0.17	0.00	0.06	0.14	0.22	0.32	0.42
13	0.31	0.25	0.17	0.11	0.05	0.00	0.42	0.33	0.22	0.13	0.06	0.00	0.18	0.39	0.27	0.16	0.07	0.00
14	0.24	0.19	0.11	0.06	0.00	0.05	0.32	0.24	0.15	0.07	0.00	0.06	0.39	0.12	0.19	0.09	0.00	0.08
15	0.17	0.12	0.06	0.00	0.06	0.11	0.22	0.15	0.07	0.00	0.07	0.14	0.27	0.19	0.04	0.00	0.09	0.16
16	0.11	0.06	0.00	0.06	0.12	0.17	0.13	0.07	0.00	0.07	0.16	0.22	0.16	0.09	0.00	0.04	0.18	0.26
17	0.05	0.00	0.05	0.11	0.19	0.24	0.06	0.00	0.07	0.15	0.24	0.32	0.07	0.00	0.09	0.18	0.11	0.41
18	0.00	0.05	0.10	0.17	0.25	0.31	0.00	0.06	0.13	0.22	0.33	0.42	0.00	0.08	0.16	0.26	0.41	0.17

Figure 18 Maximum pitch angles in degree for the scenarios of two corrosion holes with a diameter of 300mm located at different ballast tanks.

tank No.	1	2	3	4	5	6	7	8	9	10	11	12	13	14	15	16	17	18
1	0.55	1.44	1.34	1.26	1.18	1.12	0.68	0.64	0.60	0.57	0.54	0.51	0.02	0.02	0.02	0.01	0.01	0.01
2	1.44	0.58	1.41	1.36	1.31	1.26	0.69	0.66	0.63	0.61	0.59	0.57	0.02	0.01	0.01	0.01	0.01	0.01
3	1.34	1.41	0.54	1.26	1.24	1.22	0.59	0.58	0.57	0.56	0.56	0.55	0.02	0.02	0.02	0.02	0.02	0.02
4	1.26	1.36	1.26	0.56	1.34	1.35	0.58	0.58	0.59	0.59	0.60	0.61	0.01	0.01	0.01	0.01	0.02	0.02
5	1.18	1.31	1.24	1.34	0.58	1.54	0.57	0.59	0.61	0.63	0.66	0.68	0.01	0.01	0.02	0.02	0.02	0.02
6	1.12	1.26	1.22	1.35	1.54	0.55	0.51	0.54	0.56	0.60	0.64	0.67	0.01	0.02	0.02	0.02	0.02	0.02
7	0.68	0.69	0.59	0.58	0.57	0.51	0.00	0.00	0.00	0.00	0.00	0.00	0.83	0.78	0.73	0.68	0.64	0.61
8	0.64	0.66	0.58	0.58	0.59	0.54	0.00	0.00	0.00	0.00	0.00	0.00	0.81	0.78	0.75	0.72	0.69	0.67
9	0.60	0.63	0.57	0.59	0.61	0.56	0.00	0.00	0.00	0.00	0.00	0.00	0.72	0.71	0.70	0.69	0.68	0.67
10	0.57	0.61	0.56	0.59	0.63	0.60	0.00	0.00	0.00	0.00	0.00	0.00	0.67	0.68	0.69	0.70	0.71	0.72
11	0.54	0.59	0.56	0.60	0.66	0.64	0.00	0.00	0.00	0.00	0.00	0.00	0.67	0.69	0.72	0.75	0.78	0.81
12	0.51	0.57	0.55	0.61	0.68	0.67	0.00	0.00	0.00	0.00	0.00	0.00	0.61	0.65	0.68	0.73	0.78	0.84
13	0.02	0.02	0.02	0.01	0.01	0.01	0.83	0.81	0.72	0.67	0.67	0.61	0.72	1.90	1.79	1.67	1.56	1.47
14	0.02	0.01	0.02	0.01	0.01	0.02	0.78	0.78	0.71	0.68	0.69	0.65	1.90	0.75	1.87	1.78	1.71	1.64
15	0.02	0.01	0.02	0.01	0.02	0.02	0.73	0.75	0.70	0.69	0.72	0.68	1.79	1.87	0.71	1.71	1.68	1.66
16	0.01	0.01	0.02	0.01	0.02	0.02	0.68	0.72	0.69	0.70	0.75	0.73	1.67	1.78	1.71	0.68	1.68	1.71
17	0.01	0.01	0.02	0.02	0.02	0.02	0.64	0.69	0.68	0.71	0.78	0.78	1.56	1.71	1.68	1.68	0.71	2.04
18	0.01	0.01	0.02	0.02	0.02	0.02	0.61	0.67	0.67	0.72	0.81	0.84	1.47	1.64	1.66	1.71	2.04	0.69

Figure 19 Maximum roll angles in degree for the scenarios of two corrosion holes with a diameter of 300mm located at different ballast tanks.

5 Automatic Ballasting with Corrosion-induced Holes

5.1 Case description

In this chapter we will be focusing on the maximum pitch and roll angles experienced by the floating dock under the influence of automatic ballast control. Just like the case without ballast control, the draught when a vessel is atop the floating dock is 3.5 m. However, the dock experiences a tilt when one or two ballast tanks happens to have a corrosion induced hole. The present study comprises of two main scenarios: one regarding ballasting operation and the other regarding de-ballasting operation. In the case of the ballasting operation we also have two scenarios: one is that a corrosion-induced hole with different diameters occurs in one single ballast tank during the ballasting operation and another is that two ballast tanks have corrosion-induced holes of 300mm each. For the de-ballasting case, the scenario involves two ballast tanks which have corrosion-induced holes of 300mm each.

5.2 Results and discussions

5.2.1 Scenario of one corrosion-induced hole

The time-step sensitivity study of the draught, pitch and roll angles during the automatic ballasting with the corrosion induced hole located at Tank No. 01 is performed and this is shown in Figure 20. The hole diameter is 50mm. Three time-steps of $\Delta t = 1s$, $0.5s$ and 0.25s are tested, and the results for the draught and pitch angles exhibit good agreement across all time-steps. However, some discrepancies were observed in the time history of the roll angle, particularly when using a time-step of 1s. The differences between the results for time-steps of 0.5s and 0.25s are observed to be smaller, and a time-step of 0.5s was selected for further calculations to achieve a balance between the computational cost and the accuracy.

An important factor in controlling the floating dock's ballasting operations is the tank fraction. In order to achieve the appropriate stability or trim of the floating dock, it determines how much ballast water needs to be added to or removed from the tank. Figure 21 shows a comparison between tank No.01 without a corrosion-induced hole and other scenarios with different hole diameters. The hole diameter varries from 50mm to 300mm. The finding shows that when tank No. 01 has a hole, initially, the amount of ballast water increases more slowly than that when tank No.

01 doesn't have a hole. The tank with the hole eventually reaches an equilibrium point when the flow rate of ballast water becomes zero.
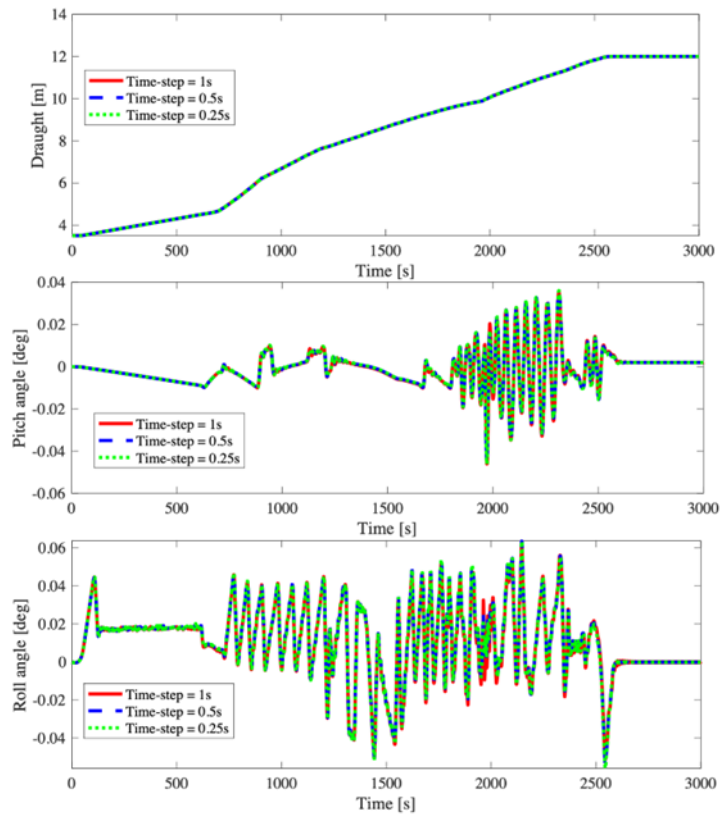
Figure 20 Time-step sensitivity study of the draught, pitch and roll angles during the automatic ballasting with the corrosion-induced hole located at Tank No. 01.
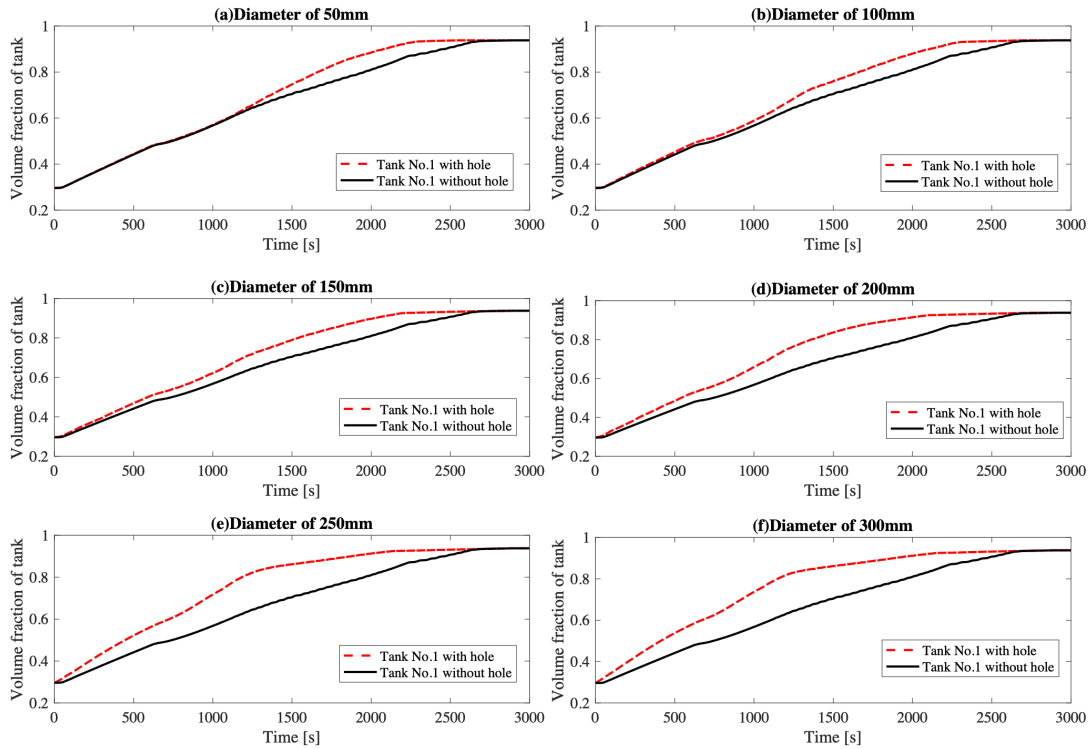
Figure 21 Tank fractions associated with different scenarios.

Figures 22 and 23 present a comparative analysis of the roll and pitch angles for Tank No.01 in various scenarios, specifically examining the effect of the hole diameters by comparing the normal case without hole. The presence of an automatic ballast control is crucial for maintaining the stability of the docking system. Without it, the dock will eventually capsize when larger roll or pitch angles are experienced. Across all the cases, the maiximum pitch and roll angles are controlled within the ranges of [-0.05deg, 0.05deg] and [-0.05deg, 0.1deg], respectively. These comparisons indicate that the inflow of water into the tank is controlled and regulated effectively.

The automatic ballast control system consistently works to maintain the stability of the dock. Additionally, it is observed that tanks with larger hole diameters initially experience a negative roll or pitch angle, primarily due to the higher volume of water rushing into the tank compared to tanks with smaller hole diameters.
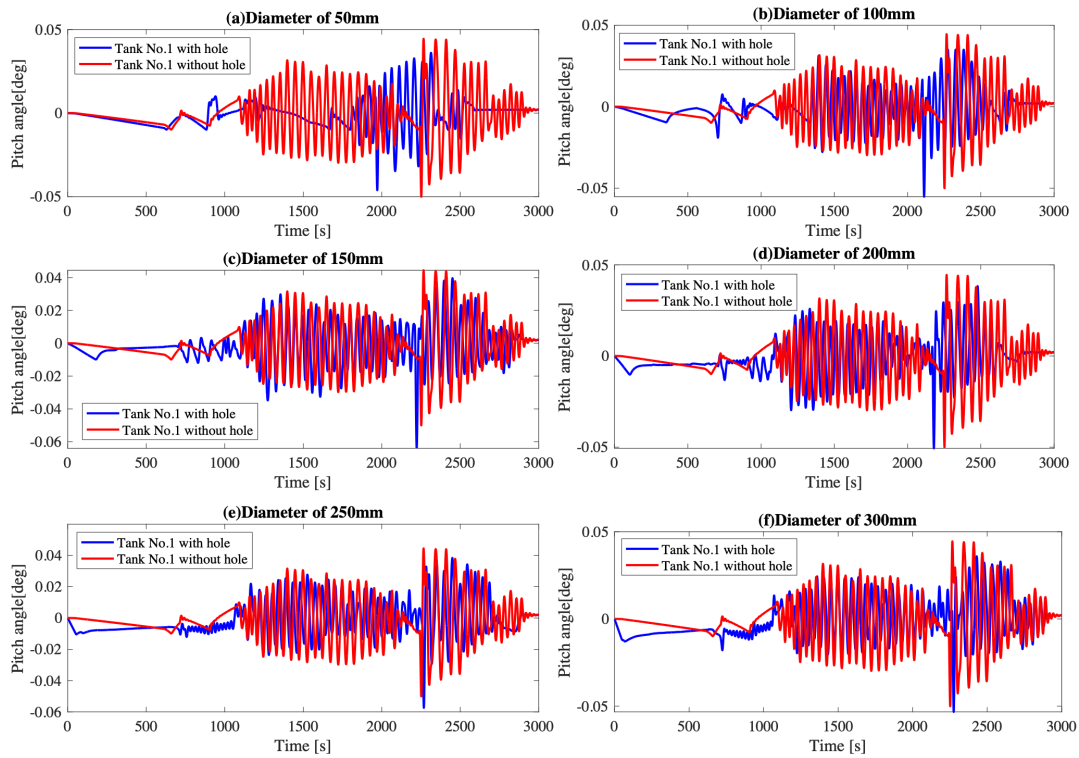
Figure 22 Comparison of of the pitch angles between the ballasting with and without corrosion-induced hole with different diameters.
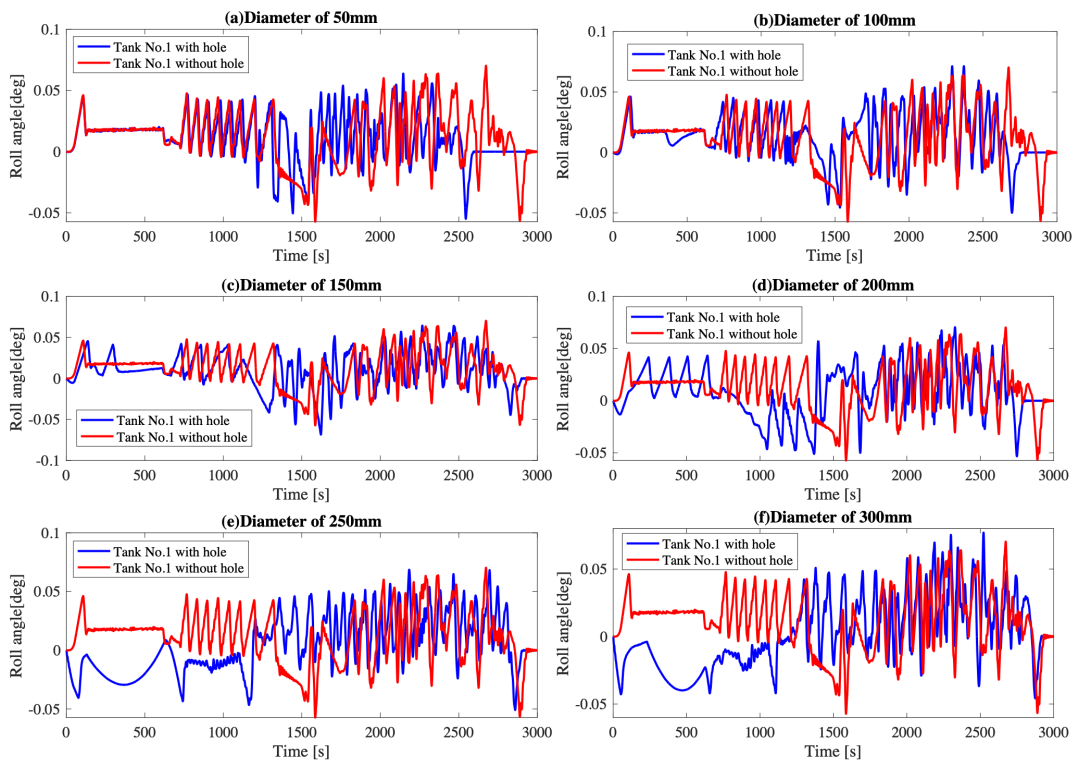
Figure 23 Comparison of of the roll angles between the ballasting with and without corrosion-induced hole with different diameters.

Figure 24 shows the comparison of flow rates through the holes between the automatic ballasting with corrosion-induced holes with diameters of 50mm and 300mm. The flow rate through the 50mm hole is relatively small as compared to the scenario with a diameter of 300mm. The flow rate through the hole with a diameter of 300mm finally changes to an up-and-down pattern. It be caused by the tank reaching its capacity and filling up. When the tank is full, any extra liquid entering the tank will flow out through the hole since there is no more room in the tank for the incoming sea water.
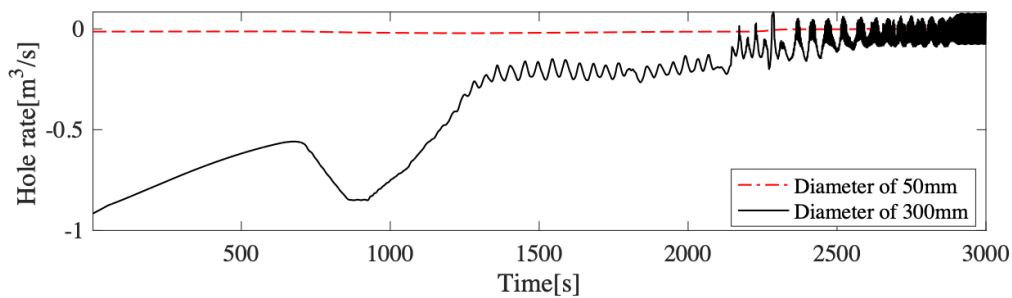
Figure 24 Comparison of the flow rates through the holes between the automatic ballasting with corrosion-induced holes with diameters of 50mm and 300mm.

Figure 25 shows comparisons of the valve opening angles at Tank No. 01 between the automatic ballasting with corrosion-induced holes with diameters of 50mm and 300mm. The valve opening angle for the case with a 50mm hole reaches 90deg initially and then decreases to 70deg as the seawater emerges the deck of the floating dock. For the case of with a 300mm hole, the valve opening angle is lower than that of the case with a 50mm hole. Figure 26 shows the comparison of flow rates at Tank No. 01 between the automatic ballasting with corrosion-induced holes with diameters of 50mm and 300mm. The flow rate includes the contribution of the tank valve and the corrosion-induced hole. That is why the flow rate of the case with a 300mm is larger than that of the case with a 50mm in the first 1000s, though the valve opening angle is smaller.

Figures 27 and 28 present comparisons of the roll and pitch angles at Tank No. 01 between the automatic ballasting with corrosion-induced holes with diameters of 50mm and 300mm. In both figures, we can observe initial negative pitch and roll angles for the 300mm hole, indicating that it accommodates a larger volume of water in the tank compared to the 50mm hole. Additionally, it's noticeable that the pitch and roll angles of the case with a 50mm hole approach to 0deg sooner than that of the case with a 300mm hole. This suggests that the tank stabilizes or returns to an even

position more quickly with the smaller hole, implying that the 50mm hole has a less pronounced impact on the tank's pitch and roll angles compared with the 300mm hole.

Figure 25 Comparisons of the valve opening angles at Tank No. 01 between the automatic ballasting with corrosion-induced holes with diameters of 50mm and 300mm.

Figure 26 Comparison of the flow rates at Tank No. 01 between the automatic ballasting with corrosion-induced holes with diameters of 50mm and 300mm.

Figure 27 Comparison of the roll angles at Tank No. 01 between the automatic ballasting with corrosion-induced holes with diameters of 50mm and 300mm.
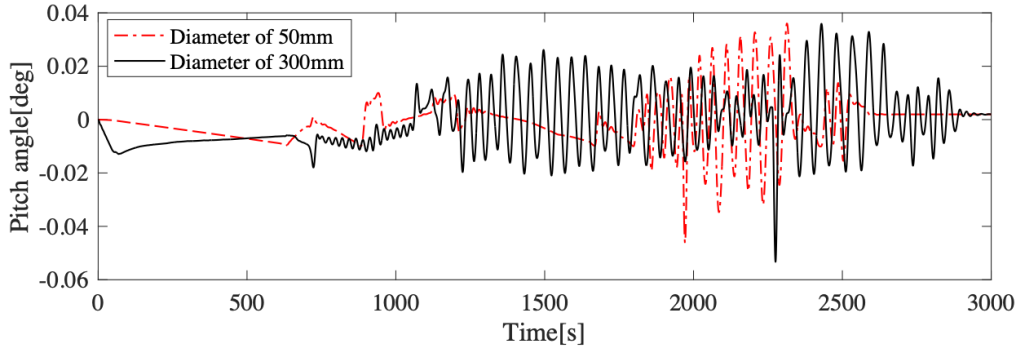
Figure 28 Comparison of the pitch angles at Tank No. 01 between the automatic ballasting with corrosion-induced holes with diameters of 50mm and 300mm.
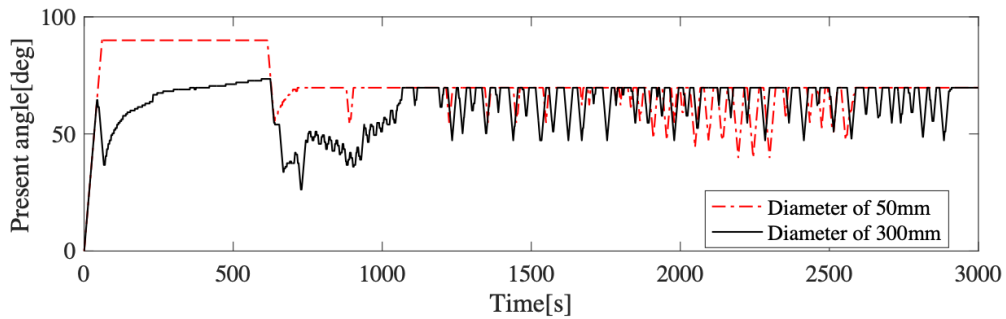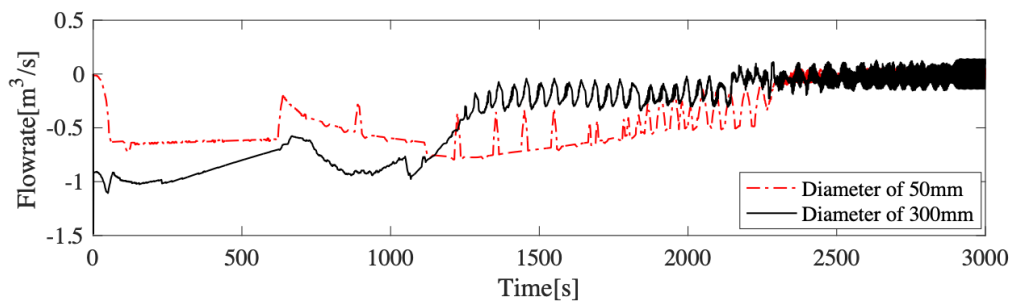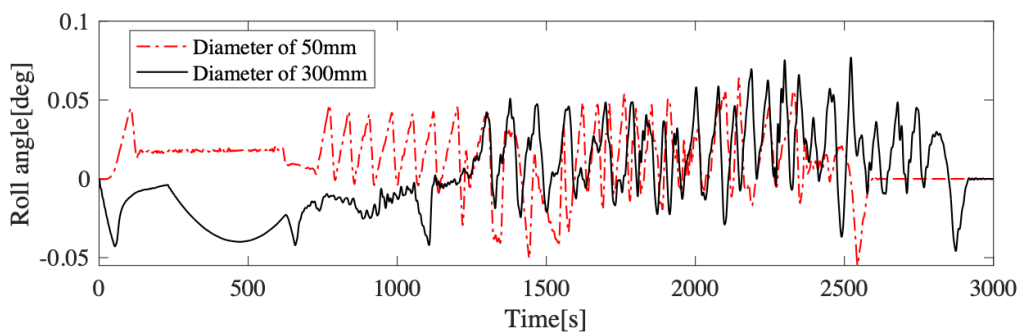
5.2.2 Scenario of two corrosion-induced holes

Figures 29 and 30 shows the maximum pitch and roll angles of the floating dock during the ballasting with corrosion-induced holes located at two different tanks. The results of the one-hole cases are also given for comparison. Across all the one- and two-hole cases, the maximum pitch and roll angles are 0.09deg and 0.13deg, respectively. The present modified P-controller can effectively stabilize the pitch and roll angles during the ballasting with one or two corrosion induced holes at the ballast tanks.

Tank No. [-]	1	2	3	4	5	6	7	8	9	10	11	12	13	14	15	16	17	18
1	0.08	0.05	0.08	0.04	0.06	0.06	0.06	0.06	0.06	0.06	0.05	0.06	0.06	0.06	0.07	0.08	0.07	0.06
2	0.05	0.04	0.08	0.07	0.08	0.07	0.09	0.07	0.06	0.06	0.07	0.05	0.05	0.07	0.05	0.06	0.07	0.07
3	0.08	0.08	0.07	0.08	0.07	0.08	0.08	0.06	0.09	0.05	0.05	0.07	0.04	0.06	0.05	0.07	0.07	0.07
4	0.04	0.07	0.08	0.05	0.06	0.07	0.07	0.07	0.07	0.08	0.09	0.05	0.05	0.05	0.06	0.07	0.07	0.08
5	0.06	0.08	0.07	0.06	0.05	0.08	0.08	0.05	0.08	0.04	0.07	0.07	0.05	0.04	0.06	0.09	0.09	0.07
6	0.06	0.07	0.08	0.07	0.08	0.06	0.08	0.08	0.08	0.07	0.07	0.06	0.07	0.07	0.06	0.08	0.07	0.09
7	0.06	0.09	0.08	0.07	0.08	0.08	0.07	0.08	0.06	0.06	0.07	0.05	0.05	0.07	0.05	0.05	0.05	0.05
8	0.06	0.07	0.06	0.07	0.05	0.08	0.08	0.07	0.08	0.08	0.06	0.06	0.06	0.07	0.06	0.09	0.09	0.06
9	0.06	0.06	0.09	0.07	0.08	0.08	0.06	0.08	0.06	0.05	0.06	0.06	0.06	0.08	0.04	0.08	0.09	0.07
10	0.06	0.06	0.05	0.08	0.04	0.07	0.06	0.08	0.05	0.08	0.05	0.06	0.05	0.06	0.06	0.08	0.09	0.07
11	0.05	0.07	0.05	0.09	0.07	0.07	0.07	0.06	0.06	0.05	0.08	0.06	0.05	0.07	0.06	0.05	0.06	0.06
12	0.06	0.05	0.07	0.05	0.07	0.06	0.05	0.06	0.06	0.06	0.06	0.07	0.05	0.05	0.06	0.07	0.08	0.06
13	0.06	0.05	0.04	0.05	0.05	0.07	0.05	0.06	0.06	0.05	0.05	0.05	0.04	0.08	0.05	0.07	0.06	0.07
14	0.06	0.07	0.06	0.05	0.04	0.07	0.07	0.07	0.08	0.06	0.07	0.05	0.08	0.06	0.08	0.05	0.05	0.08
15	0.07	0.05	0.05	0.06	0.06	0.06	0.05	0.06	0.04	0.06	0.06	0.06	0.05	0.08	0.08	0.06	0.09	0.07
16	0.08	0.06	0.07	0.07	0.09	0.08	0.05	0.09	0.08	0.08	0.05	0.07	0.07	0.05	0.06	0.09	0.07	0.07
17	0.07	0.07	0.07	0.07	0.09	0.07	0.05	0.09	0.09	0.09	0.06	0.08	0.06	0.05	0.09	0.07	0.05	0.07
18	0.06	0.07	0.07	0.08	0.07	0.09	0.05	0.06	0.07	0.07	0.06	0.06	0.07	0.08	0.07	0.07	0.07	0.06

Tank No. [-]

Figure 29 Maximum pitch angles in degree for the scenarios of two corrosion holes with a diameter of 300mm located at different ballast tanks.

	1	2	3	4	5	6	7	8	9	10	11	12	13	14	15	16	17	18
1	0.10	0.10	0.08	0.08	0.08	0.08	0.07	0.08	0.07	0.07	0.08	0.08	0.07	0.06	0.10	0.07	0.07	0.07
2	0.10	0.09	0.11	0.11	0.09	0.08	0.07	0.09	0.10	0.11	0.08	0.08	0.07	0.08	0.06	0.07	0.07	0.06
3	0.08	0.11	0.07	0.08	0.08	0.09	0.10	0.08	0.08	0.12	0.07	0.09	0.08	0.07	0.09	0.08	0.08	0.05
4	0.08	0.11	0.08	0.07	0.09	0.13	0.07	0.09	0.09	0.08	0.07	0.08	0.07	0.08	0.07	0.07	0.07	0.07
5	0.08	0.09	0.08	0.09	0.08	0.12	0.07	0.08	0.09	0.07	0.08	0.07	0.07	0.07	0.06	0.06	0.06	0.06
6	0.08	0.08	0.09	0.13	0.12	0.08	0.07	0.08	0.08	0.09	0.07	0.08	0.08	0.07	0.07	0.08	0.06	0.08
7	0.07	0.07	0.10	0.07	0.07	0.07	0.06	0.06	0.07	0.06	0.09	0.08	0.06	0.08	0.06	0.07	0.08	0.06
8	0.08	0.09	0.08	0.09	0.08	0.08	0.06	0.08	0.07	0.07	0.06	0.07	0.07	0.08	0.07	0.07	0.06	0.07
9	0.07	0.10	0.08	0.09	0.09	0.08	0.07	0.07	0.07	0.06	0.10	0.07	0.07	0.07	0.07	0.08	0.07	0.06
10	0.07	0.11	0.12	0.08	0.07	0.09	0.06	0.07	0.06	0.07	0.08	0.08	0.07	0.08	0.06	0.05	0.08	0.06
11	0.08	0.08	0.07	0.07	0.08	0.07	0.09	0.06	0.10	0.08	0.06	0.07	0.07	0.07	0.07	0.07	0.06	0.06
12	0.08	0.08	0.09	0.08	0.07	0.08	0.08	0.07	0.07	0.08	0.07	0.09	0.10	0.08	0.09	0.06	0.07	0.08
13	0.07	0.07	0.08	0.07	0.07	0.08	0.06	0.07	0.07	0.07	0.07	0.10	0.09	0.11	0.10	0.09	0.09	0.09
14	0.06	0.08	0.07	0.08	0.07	0.07	0.08	0.07	0.07	0.08	0.07	0.08	0.11	0.09	0.09	0.09	0.09	0.09
15	0.10	0.06	0.09	0.07	0.06	0.07	0.06	0.08	0.07	0.06	0.07	0.09	0.10	0.09	0.09	0.09	0.09	0.09
16	0.07	0.07	0.08	0.07	0.06	0.08	0.07	0.07	0.08	0.05	0.07	0.06	0.09	0.09	0.09	0.08	0.09	0.09
17	0.07	0.07	0.08	0.07	0.06	0.06	0.08	0.06	0.07	0.08	0.06	0.07	0.09	0.09	0.09	0.09	0.09	0.10
18	0.07	0.06	0.05	0.07	0.06	0.08	0.06	0.07	0.06	0.06	0.06	0.08	0.09	0.09	0.09	0.09	0.10	0.08

Tank No. [-]

Figure 30 Maximum roll angles in degree for the scenarios of two corrosion holes with a diameter of 300mm located at different ballast tanks during ballasting operation.

6 Automatic De-ballasting with Corrosion-induced Holes

6.1 Case description

In this chapter, the automatic de-ballasting with corrosion-induced holes is investigated. The diameter of the hole is fixed as 300mm based on the conclusion of Chapter 4. Unlike that of the ballasting operation where the ballast water flows into tanks by gravity, a pump will be required to suck out the water from the tanks in the case of the de-ballasting operation. During the de-ballasting, the water outside the dock goes into the specific tanks through the corrosion-induced holes, which will cause the tilting of the floating dock. This section also focuses on two scenarios of one and two corrosion-induced hole cases. The effects of the corrosion-induced holes on the control performance of the modified P-controller are investigated.

6.2 Results and discussion

Figures 31 and 32 show the maximum pitch and roll angles for the scenarios of two corrosion-induced holes with a diameter of 300mm located at different ballast tanks during de-ballasting operation. The Modified P-controller manages to keep the pitch and roll angles of more

than half of the cases within the safety ranges. Cases highlighted in red represent the severe cases where the Modified P-controller failed to ensure the stability of the floating dock. The large pitch angles occur when the two corrosion-induce hole are located at the ballast tanks belong to different groups of the ballast system and these two tanks are positioned at the fore or aft of the dock. The large pitch angles of these cases can be attributed to the extra water flow into these two tanks through the corrosion-induced holes. When the two tanks are located far away from the centre of the dock, the pitch moment resulting from the extra water in these two tanks becomes significant. The large roll angles are also experienced when the ballast tanks are far from the centre of the dock. There is an exception. For instance, in the scenarios where Tank No.01 and 13 have corrosion-induced holes, there is a large roll angle as well. This is because the water level of the port tanks are elevated due to the void filled by the pumps. As a result, Tank No. 01 is emptied faster than that of No. 13. More ballast water in Tank No.13 and less in Tank No.01 cause floating dock to experience a larger roll.

Tank No. [-]

	1	2	3	4	5	6	7	8	9	10	11	12	13	14	15	16	17	18
1	0.08	2.32	0.95	0.04	0.04	0.02	0.62	2.11	0.89	0.07	0.04	0.05	0.77	2.28	0.89	0.11	0.04	0.03
2	2.32	0.04	0.05	0.03	0.03	0.03	1.98	0.05	0.04	0.03	0.02	0.03	2.20	0.05	0.04	0.03	0.02	0.08
3	0.95	0.05	0.03	0.02	0.02	0.04	0.62	0.03	0.03	0.02	0.02	0.04	0.89	0.04	0.03	0.02	0.03	0.10
4	0.04	0.03	0.02	0.02	0.03	0.72	0.05	0.03	0.02	0.02	0.03	0.38	0.17	0.02	0.03	0.02	0.04	0.74
5	0.04	0.03	0.02	0.03	0.03	2.20	0.03	0.03	0.02	0.03	0.04	1.87	0.14	0.02	0.02	0.04	0.03	2.15
6	0.02	0.03	0.04	0.72	2.20	0.05	0.03	0.04	0.04	0.58	2.01	0.42	0.06	0.03	0.04	0.69	2.21	0.59
7	0.62	1.98	0.62	0.05	0.03	0.03	0.09	1.76	0.69	0.07	0.04	0.05	0.66	1.86	0.80	0.17	0.04	0.03
8	2.11	0.05	0.03	0.03	0.03	0.04	1.76	0.02	0.06	0.03	0.02	0.03	1.91	0.04	0.07	0.03	0.02	0.04
9	0.89	0.04	0.03	0.02	0.02	0.04	0.69	0.06	0.02	0.02	0.03	0.04	0.91	0.07	0.03	0.02	0.03	0.09
10	0.07	0.03	0.02	0.02	0.03	0.58	0.07	0.03	0.02	0.02	0.03	0.48	0.20	0.03	0.03	0.02	0.03	0.83
11	0.04	0.02	0.02	0.03	0.04	2.01	0.04	0.02	0.03	0.03	0.03	1.67	0.06	0.02	0.02	0.03	0.03	1.85
12	0.05	0.03	0.04	0.38	1.87	0.42	0.05	0.03	0.04	0.48	1.67	0.04	0.04	0.04	0.06	0.68	1.79	0.54
13	0.77	2.20	0.89	0.17	0.14	0.06	0.66	1.91	0.91	0.20	0.06	0.04	0.26	1.96	1.01	0.47	0.08	0.02
14	2.28	0.05	0.04	0.02	0.02	0.03	1.86	0.04	0.07	0.03	0.02	0.04	1.96	0.03	0.15	0.03	0.02	0.04
15	0.89	0.04	0.03	0.03	0.02	0.04	0.80	0.07	0.03	0.03	0.02	0.06	1.01	0.15	0.02	0.02	0.03	0.32
16	0.11	0.03	0.02	0.02	0.04	0.69	0.17	0.03	0.02	0.02	0.03	0.68	0.47	0.03	0.02	0.02	0.09	0.99
17	0.04	0.02	0.03	0.04	0.03	2.21	0.04	0.02	0.03	0.03	0.03	1.79	0.08	0.02	0.03	0.09	0.03	1.94
18	0.03	0.08	0.10	0.74	2.15	0.59	0.03	0.04	0.09	0.83	1.85	0.54	0.02	0.04	0.32	0.99	1.94	0.15
	1	2	3	4	5	6	7	8	9	10	11	12	13	14	15	16	17	18

Tank No. [-]

Figure 31 Maximum pitch angles in degree for the scenarios of two corrosion-induced holes with a diameter of 300mm located at different ballast tanks during de-ballasting operation.

Tank No. [-]	1	2	3	4	5	6	7	8	9	10	11	12	13	14	15	16	17	18
1	0.24	1.85	2.01	0.15	0.14	0.13	2.22	0.50	0.74	0.17	0.12	0.13	2.56	1.69	2.70	0.40	0.08	0.10
2	1.85	0.12	0.13	0.10	0.14	0.14	0.34	0.09	0.11	0.12	0.10	0.10	1.22	0.10	0.10	0.11	0.12	0.28
3	2.01	0.13	0.11	0.12	0.14	0.13	0.85	0.11	0.12	0.11	0.10	0.11	2.63	0.11	0.10	0.11	0.11	0.32
4	0.15	0.10	0.12	0.10	0.12	1.95	0.10	0.10	0.09	0.11	0.10	0.20	0.66	0.10	0.11	0.12	0.11	2.32
5	0.14	0.14	0.14	0.12	0.12	2.16	0.11	0.10	0.11	0.10	0.10	0.23	0.49	0.13	0.09	0.11	0.10	1.63
6	0.13	0.14	0.13	1.95	2.16	0.10	0.11	0.10	0.10	0.38	0.35	1.69	0.19	0.11	0.12	2.39	2.05	2.42
7	2.22	0.34	0.85	0.10	0.11	0.11	0.29	2.29	2.34	0.23	0.11	0.13	2.74	3.49	3.25	0.63	0.10	0.11
8	0.50	0.09	0.11	0.10	0.10	0.10	2.29	0.11	0.19	0.11	0.11	0.11	3.17	0.11	0.24	0.10	0.12	0.10
9	0.74	0.11	0.12	0.09	0.11	0.10	2.34	0.19	0.11	0.10	0.11	0.10	3.61	0.25	0.11	0.11	0.12	0.33
10	0.17	0.12	0.11	0.11	0.10	0.38	0.23	0.11	0.10	0.11	0.12	1.80	0.77	0.11	0.11	0.12	0.10	3.44
11	0.12	0.10	0.10	0.10	0.10	0.35	0.11	0.11	0.11	0.12	0.13	2.16	0.21	0.11	0.11	0.11	0.10	3.74
12	0.13	0.10	0.11	0.20	0.23	1.69	0.13	0.11	0.10	1.80	2.16	0.11	0.10	0.13	0.20	2.82	4.07	2.19
13	2.56	1.22	2.63	0.66	0.49	0.19	2.74	3.17	3.61	0.77	0.21	0.10	1.04	4.02	4.12	1.90	0.26	0.12
14	1.69	0.10	0.11	0.10	0.13	0.11	3.49	0.11	0.25	0.11	0.11	0.13	4.02	0.11	0.60	0.10	0.12	0.14
15	2.70	0.10	0.10	0.11	0.09	0.12	3.25	0.24	0.11	0.11	0.11	0.20	4.12	0.60	0.11	0.12	0.11	1.30
16	0.40	0.11	0.11	0.12	0.11	2.39	0.63	0.10	0.11	0.12	0.11	2.82	1.90	0.10	0.12	0.12	0.31	4.13
17	0.08	0.12	0.11	0.11	0.10	2.05	0.10	0.12	0.12	0.10	0.10	4.07	0.26	0.12	0.11	0.31	0.11	4.95
18	0.10	0.28	0.32	2.32	1.63	2.42	0.11	0.10	0.33	3.44	3.74	2.19	0.12	0.14	1.30	4.13	4.95	0.53

Tank No. [-]

Figure 32 Maximum roll angles in degree for the scenarios of two corrosion induced-holes with a diameter of 300mm located at different ballast tanks during de-ballasting operation.

The draught, roll and pitch of the automatic ballasting with two corrosion-induced holes located at Tanks No.01 and 02 is compared with those of the case of the automatic ballasting with two corrosion-induced holes located at Tanks No.01 and 05 in Figure 33. It is observed that the case of Tank No.01 and 02 tends to have a larger pitch and roll angles. This is primarily due to the location of the tanks. Figure 34 shows the comparisons of the volume fractions of Tanks No.01, 02 and 05. Tanks No.01 and 05 in the first case is emptied faster than Tanks No.01 and 02 in the second case. Figure 35 shows the comparisons of the valve opening angles between the case of Tanks No.01 and 05 and the case of No.01 and 02. In the second case, the valve opening angles at Tanks No.01 and 02 are kept to be the maximum values to empty the ballast water. However, the Modified P-controller still cannot stabilize the pitch and roll angles of the floating dock. In the first case, the modified P-controller controls the motions of the floating dock well and the ballast water in Tanks No.01 and 05 are de-ballasted much faster than that of the first case. The valve opening angles at Tank No.01 is kept to be the maximum value, while that of Tank No.05 maintains close to 35deg, which is the minimum valve opening angle during the de-ballasting operation.
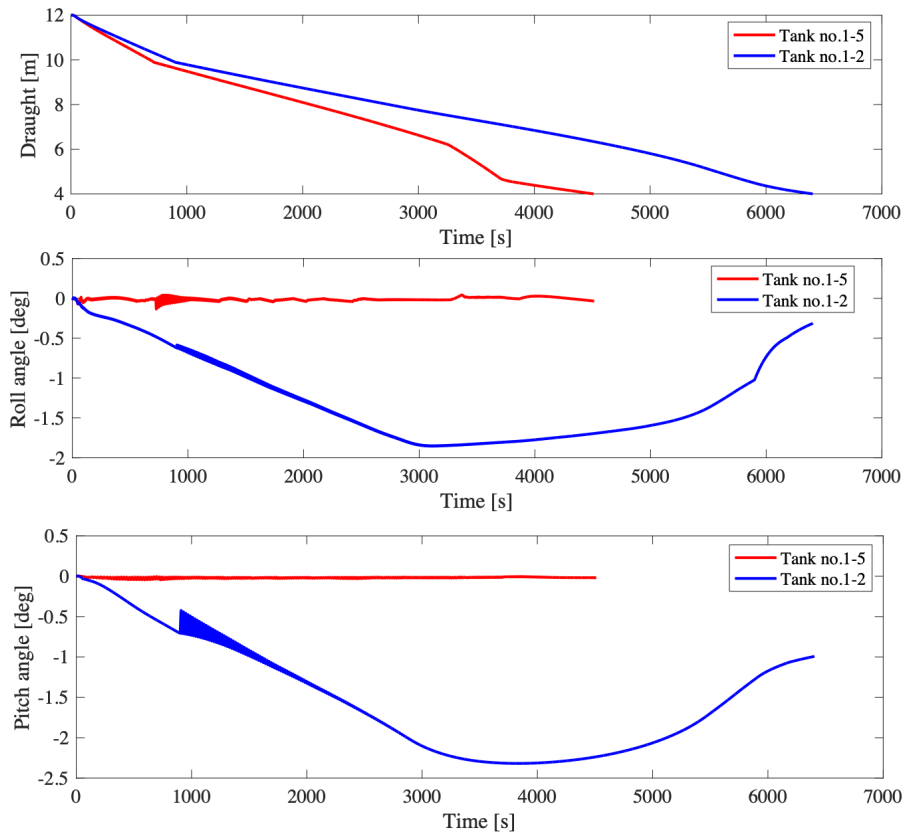
Figure 33 Comparisons of the draught, roll and pitch of the floating dock when different ballast tanks have corrosion-induced holes with diameter of 300mm during de-ballasting operation.
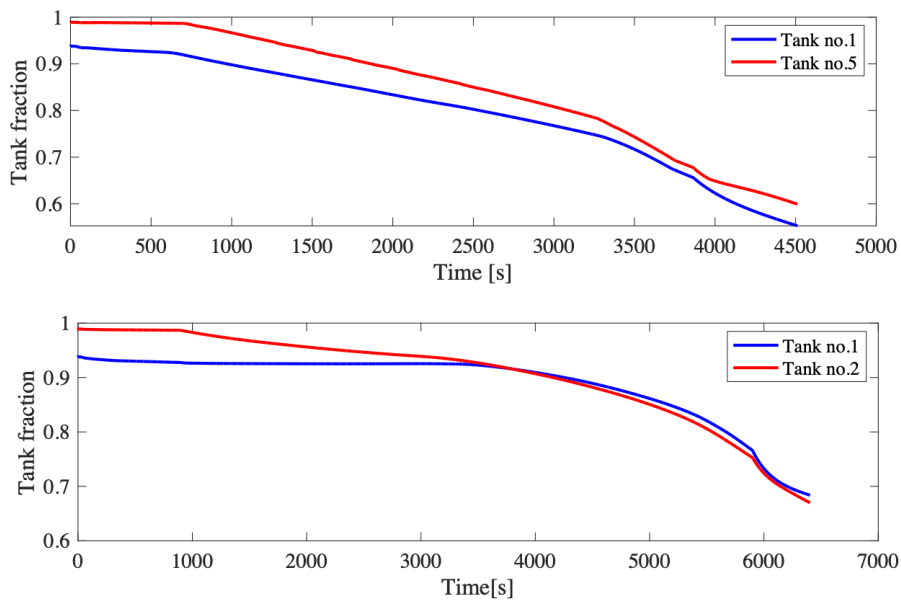

Figure 34 Comparisons of the volume fractions of Tanks No.01, 02 and 05 when different ballast tanks have corrosion-induced holes with diameter of 300mm during de-ballasting operation.
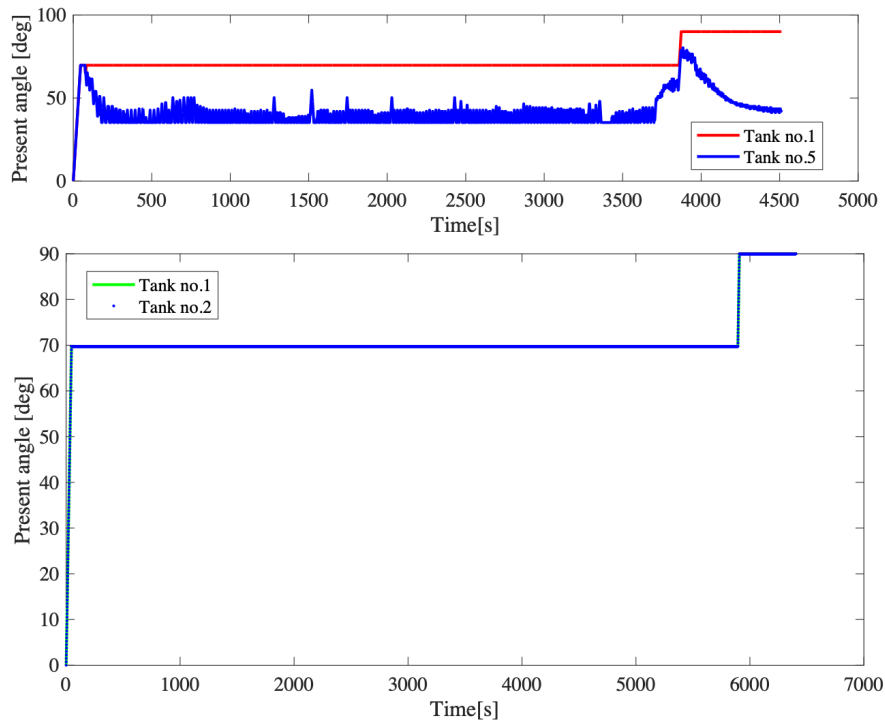
Figure 35 Comparisons of the valve opening angles between the case of Tanks No.01 and 02 and the case of Tanks No.01 and 05.

7 Conclusions

The dynamic responses of a floating dock under corrosion-induced accidents are studied using a numerical method. The numerical model is proposed based on a 6-DOF model which is for the calculation of the dock's motions in six degrees of freedom, a hydrostatic force model developed using the Archimedes law and a strip theory along the longitudinal direction, a hydrodynamic force model which focuses on the effects of added mass and dynamic damping, and a hydraulic model which is for the hydraulic calculation of the ballast water system. The automatic control of the ballast system is emplemented using a modified P-controller. The effects of the corrosion-induced holes on the stability of the floating dock and the automatic ballast control during the ballasting and de-ballasting operations are investigated and the main results are listed below:

(a) For the corrosion-induced ballasting, the maximum pitch and roll angles experienced by the floating dock during ballasting operation are 0.18 degrees and 0.72 degrees respectively when there is one hole located at one tank. The maximum pitch and roll angles become 0.42 degrees and 2.04 degrees respectively when there are two holes located at different tanks.

(b) For the automatic ballasting corrosion-induced holes, the present modified P-controller can maintain the pitch and roll angles of the floating dock within small ranges though with two corrosion-induced holes with a diameter of 300mm located at different ballast tanks.

(c) For the automatic de-ballasting corrosion-induced holes, the maximum pitch and roll angles during a de-ballasting operation become 2.32 degrees and 4.95 degrees respectively when there are two holes located at different tanks.

This above analysis not only emphasizes potential hazards but also presents an opportunity for the maritime sector to enhance safety, operational efficiency, and environmental responsibility.

Reference

[1] X.-L. and Y. Q. and T. J. Shan, "Risk management of mooring operation of floating dock," *Journal of Tianjin University Science and Technology*, vol. 42, pp. 335--339, 2009.

[2] M. El-Maadawy, M. M. Moustafa, H. S. El-Kilani, and A. A. Tawfeek, "PORT-SAID ENGINEERING RESEARCH JOURNAL Structural Safety Assessment of a Floating Dock during Docking Operation," 2018.

[3] A. Wankhede, "'Dry Docks, Types of Dry Docks & Requirements for Dry Docks',." Accessed: Sep. 01, 2023. [Online]. Available: https://www.marineinsight.com/guidelines/dry-dock-types-of-dry-docks-requirements-for-dry-dock/

[4] The Maritime Executive, "The largest floating dry dock in the baltic states." 2023. [Online]. Available: https://maritime-executive.com/features/the-largest-floating-drydock-in-the-baltic-states

[5] AqualisBraemar Technical Services Ltd:, "Floating docks and their operating hazards." Accessed: Jun. 14, 2023. [Online]. Available: https://www.shipownersclub.com/aqualisbraemar-technical-services-ltd-floating-docks-and-their-operating-hazards/

[6] T. Morra, "The Evolutionary Development of Floating Dry Docks," East Carolina University, East Carolina, 2011.

[7] W. M. Benkert and National Research Council, *Controlling Hydrocarbon Emissions from Tank Vessel Loading*. National Academies Press, 1987.

[8] M. Voytenko, "Floating dock with 2 ships inside broke in two, crane collapsed, ships taking on water," 2019. [Online]. Available: https://www.fleetmon.com/maritime-news/2019/25801/floating-dock-2-ships-inside-broke-two-crane-colla/.

[9] M. El-Maadawy, M. M. Moustafa, H. S. El-Kilani, and A. A. Tawfeek, "PORT-SAID ENGINEERING RESEARCH JOURNAL Structural Safety Assessment of a Floating Dock during Docking Operation," 2018.

[10] Yu Dykhta, L., V. Kozlyakov. "On The Floating Dock's Dynamical Behaviour Under Wind Squall In A Seaway." 1986.

[11] M. Tukan, B. J. Camerling, M. T. Afifudin, and Hozairi, "Decision Support System for Determining Floating Dock Locations in Maluku Islands Using AHP-TOPSIS," *Journal of*

Physics: Conference Series, Institute of Physics Publishing, Jul. 2020. DOI: 10.1088/1742-6596/1577/1/012001.

[12] J. K. Paik, A. K. Thayamballi, Y. Il Park, and J. S. Hwang, "A time-dependent corrosion wastage model for seawater ballast tank structures of ships," *Corros Sci*, vol. 46, no. 2, pp. 471–486, 2004, DOI: 10.1016/S0010-938X(03)00145-8.

[13] N. M. Noor and N. Yahaya, Noor, N. M., & Yahaya, N. (2006). "Statistical Analysis of Seawater Ballast Tank Corrosion Data." In Proceeding of the 6th Asia-Pacific Structural Engineering and Construction Conference (APSEC 2006), Kuala Lumpur, Malaysia (pp. E25-E33).

[14] American Society for Testing and Materials (ASTM), "G46-94, Standard guide for examination and evaluation of pitting corrosion," *ASTM International: West Conshohocken, PA*, 2003.

[15] Ballast and corrosion control Ocean Saver, "About Corrosion and Ballast Water Treatment Systems Two IMO initiatives relating to Ballast Water are coming into force." Accessed: Sep. 27, 2023. [Online]. Available:
http://www.atenanazionale.it/sezioni/napoli/2011/20110119shortaboutcorrosion.pdf

[16] R. E. Heger, "Floating dry dock accidents involving transverse bending failure of the pontoon." In RINA International Conference: Drydocks, launching & shiplift, 2003.

[17] Offshore technology, "Five biggest oil spills lessons." Accessed: Sep. 25, 2023. [Online]. Available: https://www.offshore-technology.com/features/five-biggest-oil-spills-lessons/?cf-view&cf-closed

[18] F. Wetenschappen, "Associatiefaculteit Nautische Wetenschappen corrosion in ballast tanks on board of merchant vessels."

[19] Interreg2seas, "Seeking out corrosion - before it is too late." 2023. [Online]. Available: https://www.interreg2seas.eu/nl/SOCORRO

[20] G. Koch, M. Brongers, N. Thompson, Y. Virmani, and J. Payer, "Corrosion Cost and Preventive Strategies in the United States," Jan. 2001.

[21] K. De Baere, H. Verstraelen, P. Rigo, S. Van Passel, S. Lenaerts, and G. Potters, "Reducing the cost of ballast tank corrosion: Aneconomic modeling approach," *Marine Structures*, vol. 32, pp. 136–152, Jul. 2013, doi: 10.1016/j.marstruc.2012.10.009.

[22] Det Norske Vertias(DNV), "Rules for Classification–Ships," 1998.

[23] De Baere, Kris, H. Verstraelen, L. Lemmens, S. Lenaerts, and G. Potters. "In situ study of the parameters quantifying the corrosion in ballast tanks and an evaluation of improving alternatives." In NACE CORROSION, pp. NACE-11419. NACE, 2011.

[24] P. Hancock, "Hordafor." 2023. [Online]. Available: https://pelagia.com/cm/hordafor/

[25] M. Voytenko, "Floating dock sank repair yard in Szczecin," 2018. [Online]. Available: https://www.fleetmon.com/maritime-news/2018/21355/flotaing-dock-sank-ship-repair-yard-szczecin/

[26] M., M., Bringslid. A., N., Olsen, "Danish cantilever dock collapses leaving fishing boat trapped," 2018. [Online]. Available: https://salmonbusiness.com/danish-cantilever-dock-collapse-leaving-fishing-boat-trapped-inside/

[27] Mfame Team. "Floating Dock Collapsed, One Ship Blocked", 2018,. [Online]. Available: https://mfame.guru/watch-floating-dock-collapsed-one-ship-blocked/."

[28] S. Rainsford, "Russian aircraft carrier Admiral Kuznetsov damaged by crane," 2018,. [Online]. Available: https://www.bbc.com/news/world-europe-46030113.

[29] National Transportation Safety Board (NTSB), Marine Accident Brief Dockside Capsizing and Sinking of Towing Vessel Invader and Dry Dock #3," 2012.

[30] Mercopress, "Ships sink in Montevideo Port dock collapse." Accessed: Sep. 25, 2023. [Online]. Available: https://en.mercopress.com/2022/12/09/ships-sink-in-montevideo-port-dock-collapse

[31] W. Belay, "Comparative study on global motion characteristics of rectangular and circular columns semi submersible," Faculty of Science and Technology, Master's thesis, University of Stavanger, Norway, 2015.

[32] S. K. Chakrabarti, "Handbook of Offshore Engineering Volume I 2005 Elsevier," 2005. [Online]. Available: www.bookaid.org

[33] J. Le, B. Børkja, "Dynamic Analysis of Floating Dock Structures," NTNU, Trondheim, 2015.

[34] A. H. Techet, *Hydrodynamics*. Cambridge , Massachusetts , United States, 2005. Accessed: Oct. 11, 2023. [Online]. Available: https://ocw.mit.edu/courses/2-016-hydrodynamics-13-012-fall-2005/6124a1fd14e811d9ea753f85e0dfc8d0_2005reading6.pdf

[35] N. J. Newman "Marine Hydrodynamics," 2017. Accessed: Oct. 12, 2023. [Online]. Available:https://home.hvl.no/ansatte/gste/ftp/MarinLab_files/Litteratur/Marine_Hydrodynamics_Newman_2018.pdf

[36] P. U. P. A. Gilbert, W. Haeberli, P. Davidovits, G. Rhodes, G. M. Mccracken, and P. Stott, "Complementary Science Series ACADEMIC PRESS 2008-To be published Physics in the

Arts (Full Edition) Edition Crystallography Made Crystal Clear, Third Edition Introduction to Quantum Mechanics," 2003. [Online]. Available: www.books.elsevier.com

[37]   Rose-Hulman.edu, "Appendix A-Mass Moments of Inertia." Accessed: Oct. 12, 2023. [Online]. Available: https://www.rosehulman.edu/ES204/PDFs/Appendix_from_Mechanical_Systems_Book.pdf

[38]   N. Salvesen, E. O. Tuck, O. M. Faltinsen, "Ship Motions and Sea Loads," 1970.

[39]   J. Gerritsma and W. Beukelman, "Analysis of the modified strip theory for the calculation of ship motions and wave bending moments," Delft, 1967.

[40]   S. Baso, S. Asri, L. B. Bochary, L. Pratama. "New Strip Theory Approach to Ship Motions Prediction." Inovasi Teknologi Kelautan. 2013.

[41]   P. J. Bandyk, "A body-exact strip theory approach to ship motion computations." Doctors thesis, University of Michigan. 2009.

[42]   J. N. Newman, R. Timman, "The Coupled Damping Coefficients of a Symmetric Ship", Journal of ship research, 6(01), pp.1-7.

[43]   J.,N., Newman "A linearized theory for the motion of a thin ship in regular waves," Doctors thesis, Massachusetts Institute of Technology (MIT), 1960.

[44]   Y. T. Fan. "Time-Domain non-linear strip theory for ship motion", Doctors thesis, University of Southampton, 2004.

[45]   O. M. Faltinsen, "Numerical solutions of transient nonlinear free-surface motion outside or inside moving bodies.," in Proceedings of the second international conference on numerical ship hydrodynamics, Berkeley, California, USA, 1977.

[46]   D. Matulja, M. Sportelli, C. Guedes Soares, Prpić-Oršić . "Estimation of Added Resistance of a Ship in Regular Waves," Brodogradnja: Teorija i praksa brodogradnje i pomorske tehnike, 2011, 62(3), pp.259-264.

[47]   O. M. Faltinsen, "Wave induced motions and loads on ships. Theory and numerical methods," Paper presented at UETP Course on New Techniques for Assesseing and quantifying vessel stability ane seakeeping qualities, March 1993., 1993. Accessed: Oct. 09, 2023. [Online]. Available: http://resolver.tudelft.nl/uuid:2e03ef83-d023-41aa-9ca7-d90450ef14c5

[48]   Elprocus, "What is a PID controller: Working & its Application." Accessed: Oct. 15, 2023. [Online]. Available: https://www.elprocus.com/the-working-of-a-pid-controller/

[49]   N. Mehta, D. Chauhan, S. Patel, and S., Mistry, "Design of HMI Based on PID Control of Temperature," International Journal of Engineering Research and, vol. V6, no. 05, May 2017, doi: 10.17577/IJERTV6IS050074.

[50]   H., Schaub, J., L., Junkins. "Analytical Mechanics of Space Systems. American Institute of Aeronautics and Astronautics," Inc., Reston, VA, pp. 23,77-123, 2003.

[51]   W. Pabst, "Theory of the landing impact of seaplanes," National Advisory Council for Aeronautics (NACA) Technical Memorandum No.580, Washington, USA, 1930.

[52]   Det Norske Vertias(DNV), *"DNV* Recommended Practice DNV-RP-C205:Environmental conditions and environmental loads." 2012.

[53]   X. Wen, A. Garcia Conde, J. Zhang, M. C. Ong. "Numerical Study on the Automatic Ballast Control of a Floating Dock." ASME. J. Offshore Mech. Arct. Eng. August 2024; 146(4): 041401. https://doi.org/10.1115/1.4064014

[54]   Eurotorc, "Butterfly valve engineering data." Accessed: Sep. 16, 2023. [Online]. Available: https://www.eurotorc.com/butterfly-valve-engineering-data.html.

[55] J. Zhang, X. Wen, M. C. Ong, "Development of a floating dock numerical model and the ballast water distribution strategy", Proceedings of the 42nd International Conference on Offshore Mechanics and Arctic Engineering (OMAE2023). American Society of Mechanical Engineers, Melbourne, Australia, (Vol. 86878, p. V005T06A068). June 11-16, 2023.